



Erythrocyte–cancer hybrid membrane-coated reduction-sensitive nanoparticles for enhancing chemotherapy efficacy in breast cancer



Somayeh Rezaei^a, Raimundo Fernandes de Araújo Júnior^{a,b,c,*}, Isadora Luisa Gomes da Silva^c, Timo Schomann^{a,d}, Christina Eich^{a,**}, Luis J. Cruz^{a,**}

^a Translational Nanobiomaterials and Imaging (TNI) Group, Department of Radiology, Leiden University Medical Center, 2333 ZA Leiden, the Netherlands

^b Postgraduate Program in Health Science, Federal University of Rio Grande do Norte (UFRN), Natal 59064-720, Brazil

^c Cancer and Inflammation Research Laboratory (LAIC), Postgraduate Program in Functional and Structural Biology, Department of Morphology, Federal University of Rio Grande do Norte (UFRN), Natal 59064-720, Brazil

^d Department of Vascular Surgery, Leiden University Medical Center, 2333 ZA Leiden, the Netherlands

ARTICLE INFO

Keywords:

Reduction-sensitive nanoparticles
Chitosan
Biomimetic nanoparticles
Cancer cell membrane-coated nanoparticles
Homotypic targeting
Red blood cells
Hybrid membrane
Breast cancer

ABSTRACT

Cell-membrane-coated biomimetic nanoparticles (NPs) have attracted great attention due to their prolonged circulation time, immune escape mechanisms and homotypic targeting properties. Biomimetic nanosystems from different types of cell -membranes (CMs) can perform increasingly complex tasks in dynamic biological environments thanks to specific proteins and other properties inherited from the source cells. Herein, we coated doxorubicin (DOX)-loaded reduction-sensitive chitosan (CS) NPs with 4T1 cancer cell -membranes (CCMs), red blood cell -membranes (RBCMs) and hybrid erythrocyte-cancer membranes (RBC-4T1CMs) to enhance the delivery of DOX to breast cancer cells. The physicochemical properties (size, zeta potential and morphology) of the resulting RBC@DOX/CS-NPs, 4T1@DOX/CS-NPs and RBC-4T1@DOX/CS-NPs, as well as their cytotoxic effect and cellular NP uptake *in vitro* were thoroughly characterized. The anti-cancer therapeutic efficacy of the NPs was evaluated using the orthotopic 4T1 breast cancer model *in vivo*. The experimental results showed that DOX/CS-NPs had a DOX-loading capacity of $71.76 \pm 0.87\%$, and that coating of DOX/CS-NPs with 4T1CM significantly increased the NP uptake and cytotoxic effect in breast cancer cells. Interestingly, by optimizing the ratio of RBCMs:4T1CMs, it was possible to increase the homotypic targeting properties towards breast cancer cells. Moreover, *in vivo* tumor studies showed that compared to control DOX/CS-NPs and free DOX, both 4T1@DOX/CS-NPs and RBC@DOX/CS-NPs significantly inhibited tumor growth and metastasis. However, the effect of 4T1@DOX/CS-NPs was more prominent. Moreover, CM-coating reduced the uptake of NPs by macrophages and led to rapid clearance from the liver and lungs *in vivo*, compared to control NPs. Our results suggest that specific self-recognition to source cells resulting in homotypic targeting increased the uptake and the cytotoxic capacity of 4T1@DOX/CS-NPs by breast cancer cells *in vitro* and *in vivo*. In conclusion, tumor-disguised CM-coated DOX/CS-NPs exhibited tumor homotypic targeting and anti-cancer properties, and were superior over targeting with RBC-CM or RBC-4T1 hybrid membranes, suggesting that the presence of 4T1-CM is critical for treatment outcome.

1. Introduction

Breast cancer is one of the most lethal cancers and accounts for over 90 % of cancer-related deaths in women. A major challenge for cancer therapy today is cancer metastasis, which occurs when cancer cells separate from a primary tumor and travel to another part of the body by

blood or the lymph system [1,2]. Chemotherapy still remains the standard method of treatment for breast cancer patients who cannot undergo resection surgery [3,4], but patients often face the side effects of anti-cancer drugs due to non-selective uptake of those drugs by normal cells in healthy tissues.

Nanoparticles (NPs) have gained much attention for cancer therapy

* Correspondence to: R. F. de Araújo Júnior, Postgraduate Program in Health Science, Federal University of Rio Grande do Norte (UFRN), Natal 59064-720, Brazil.

** Corresponding authors.

E-mail addresses: s.rezaei@lumc.nl (S. Rezaei), fernandes.araujo@ufrn.br (R.F. de Araújo Júnior), c.eich@lumc.nl (C. Eich), L.J.Cruz_Ricondo@lumc.nl (L.J. Cruz).

<https://doi.org/10.1016/j.bioadv.2023.213456>

Received 7 December 2022; Received in revised form 7 April 2023; Accepted 30 April 2023

Available online 9 May 2023

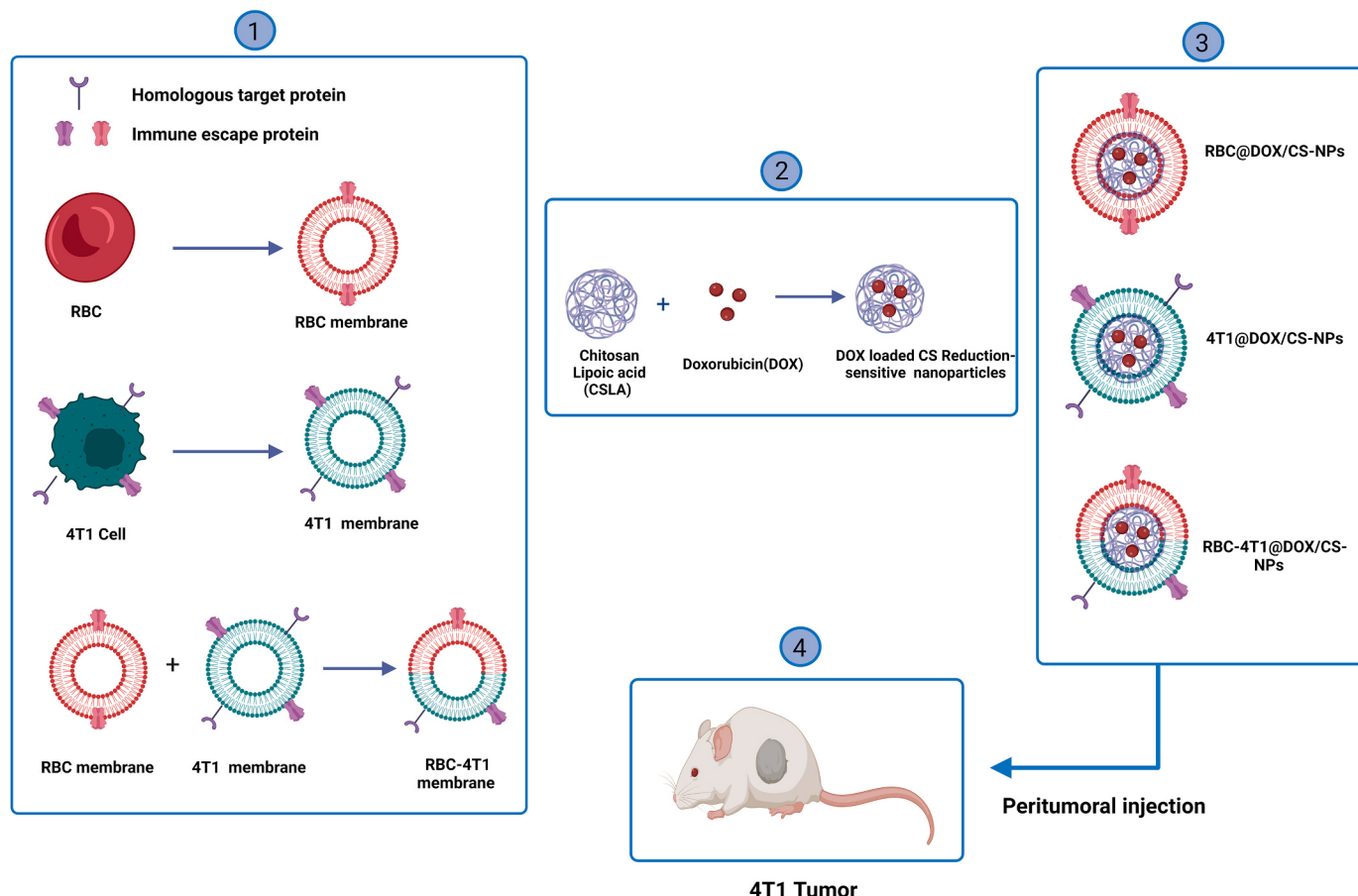
2772-9508/© 2023 The Authors. Published by Elsevier B.V. This is an open access article under the CC BY license (<http://creativecommons.org/licenses/by/4.0/>).

and diagnosis over the last decades [5]. NP-encapsulated drugs can improve drug solubility, can cross the blood vessel wall, have well adapted release kinetics, reduced side effects and increased therapeutic efficacy [6]. For cancer treatment, the use of NP platforms has increased the potency of the traditional therapeutics [7]. Depending on the NPs' physicochemical properties and surface coating, NPs that enter the blood circulation often get covered by biomolecules which form a protein corona. This can lead to changes in NP structure, function and dynamics, resulting in altered cellular recognition and uptake of the NPs [8]. The binding strength of the NPs to the protein corona depends on the NPs' physicochemical properties, such as size, charge, shape and hydrophilicity [9]. A commonly used strategy to prevent the formation of a protein corona and to increase the blood circulation time is surface modification of the NP with polyethyleneglycol (PEG) [9]. *In vitro* and *in vivo* studies support the theory that the conjugation of targeting motifs to the NP surface, including protein/peptides, folic acid, antibodies, aptamers and polysaccharides, can enhance the selectivity of cellular uptake by cancer cells and/or cytotoxicity [10].

Another form of targeted NPs, known as biomimetic NPs, can be obtained by combining synthetic NPs (as core) with a biological membrane coating (as shell). Biologically relevant surface moieties including adhesion proteins, antigens and membrane structures of source cells are transferred onto the surface of a NP by translocating entire cell membranes [7,11,12]. Recently, biomimetic NPs gained attention for therapeutic and imaging applications. In addition, cell membrane-coated NPs retain the versatility and complexity of natural cell-membranes to perform specific functions, in particular biointerfacing. Biomimetic NPs have shown target-homing abilities as well as prolonged circulation times, immune escape abilities, homologous binding properties and good biocompatibility, which are consistent with the properties of a cell

membrane [13]. Currently, most CM-based biomimetic NPs are prepared in three steps: i) membrane extraction from the source cells, ii) preparation of core NPs and iii) merging of CMs and NPs to form a membrane shell around the NP core [14]. Previous studies have shown that biomimetic NPs prevent the formation of a protein corona and represent a promising approach for the fabricating of novel nanomedicines [15]. RBCMs are one of multiple types of natural membranes, which can be coated onto NPs. However, they cannot actively target cancer cells due to a lack of targeting molecules with tumor-tropism. Conversely, CCM-derived vesicles, with inherited affinity ligands native to the source cancer cells, which can actively target cancer cells, but are prone to recognition by immune cells due to the presence of tumor antigens, and thus may not be stealthy enough to evade immune surveillance [14,16,17]. Biomimetic nanosystems can perform increasingly complex tasks in dynamic biological environments when made from different types of CMs that inherit proteins and other properties from different source cells [18]. Compared to bare NPs, hybrid membrane-coated NPs, such as RBC-platelet (PLT)-CM NPs reduce inflammation and prolong blood retention. These findings suggest that the fusion membrane-coating strategy is an effective method to increase the accumulation of NPs in tumor cells [19].

Stimuli-responsive NPs, such as pH-sensitive and glutathione (GSH)-responsive NPs, have received great attention due to their ability to achieve on-demand drug release in the tumor microenvironment (TME) [20]. Among the stimuli-responsive NPs, GSH-responsive NPs are of great interest because they slowly release drugs in blood circulation, while they excellently release drugs into the cytoplasm of cancer cells [21], where the concentration of GSH is higher than in normal tissue [22]. Chitosan (CS) is a well-known aminopolysaccharide with favorable properties, such as biocompatibility, biodegradability, low toxicity,



Scheme 1. Schematic illustration of the targeting and coating of DOX/CS-NPs by RBCMs, 4T1CMs and RBC-4TCMs for therapeutic purpose on 4T1 breast cancer.

high cationic charge and pH sensitivity, which made it widely used in biomedical applications [22].

Herein, we report the development of DOX/CS-NPs coated with 4T1, RBC and a combination of both CMs specifically for the intratumoral delivery of DOX to treat breast cancer. As shown in **Scheme 1**, the plasma membrane derived from 4T1 cells and RBCs, with its multitude of proteins, including homologous targeting proteins and immune escape proteins, bestows 4T1 and RBCMs with mimicking properties to adhere to source cells. It has been shown that intramural injection of PLT membrane-coated NPs exhibited prolonged retention at the tumor site and enhanced cellular interaction in the TME [23]. Our *in vivo* data showed that, after intratumoral administration *in vivo*, due to the homologous targeting ability of 4T1 tumor CMs, 4T1@DOX/CS-NPs could selectively accumulate in the 4T1 TME, leading to a high local concentration of DOX. In addition, RBC@DOX/CS-NPs could limit the NP uptake by macrophages. Both 4T1@DOX/CS-NPs and RBC@DOX/CS-NPs could effectively suppress the tumor growth *in situ* compared to free DOX, while to DOX/CS-NPs were less effective.

2. Material and methods

2.1. Materials and reagents

For the preparation of NPs, chitosan oligosaccharide (CSO), lipoic acid (LA), ethanol, 1-Ethyl-3-(3-dimethylaminopropyl) carbodiimide (EDC) and *N*-hydroxysuccinimide (NHS) were obtained from Sigma-Aldrich (Zwijndrecht, the Netherlands). Doxorubicin hydrochloride (DOX.HCl) was obtained from the Leiden University Medical Center Pharmacy, Leiden, the Netherlands. Cyanine5 carbocyclic acid (Cy5) was purchased from Lumiprobe, Hannover, Germany. Fetal bovine serum (FBS) and cell culture media were obtained from Gibco Laboratories (Thermo Scientific™, Waltham, Massachusetts, USA). For cell culture, 4T1 (ATCC® CRL2539™) murine breast cancer cells, mouse macrophages RAW 264.7 (ATCC® TIB-71™; mouse mononuclear macrophages), MC38 (murine colon adenocarcinoma cell), CT-26 (murine colorectal carcinoma cells) and 3 T3 (embryonic mouse fibroblast) cells were used in this study. They were purchased from the American Type Culture Collection (ATCC; Manassas, Virginia, USA). 4T1 cells were cultured and maintained in the Roswell Park Memorial Institute (RPMI) medium, supplemented with 10 % FBS and 100 U mL⁻¹ of penicillin/streptomycin (P/S). Other cell lines, *i.e.*, RAW 264.7, MC38, CT-26 and 3 T3, were cultured in complete Dulbecco's Modified Eagle Medium (DMEM) containing 10 % FBS and 100 U mL⁻¹ P/S. The cells were cultured in a humidified incubator at 37 °C with 5 % CO₂. Total RNA isolation system and CellTiter 96(R) AQueous MTS Reagent Powder were purchased from Promega (Madison, WI, USA). SnakeSkin™ Dialysis Tubing (3.5 kDa MWCO, 22 mm), high-capacity RNA-to-cDNA™ Kit, KaryoMAX™ Giemsa Staining Solution, PowerUp™ SYBR™ Green Master Mix, Lysotracker™ Deep Red, trypsin, P/S (10,000 U mL⁻¹), and FBS were purchased from Thermo Scientific™ (Waltham, MA, USA). Anti-mouse CD163-PerCP-eFluor™ 710 (Clone TNKUPJ), anti-mouse CD68-FITC (clone FA-11) and anti-mouse CD86-FITC (clone GL1) were obtained from eBioscience (San Diego, CA, USA). Anti-NF-κB (clone F-6) was purchased from Santa Cruz Biotechnology (Dallas, TX, USA). TRIzol was purchased from Invitrogen (Thermo Scientific™, Waltham, MA, USA). Biotinylated pan-specific universal secondary antibody and streptavidin/HRP-conjugated antibody were purchased from Vector Labs (Vicbio Biotechnology Co., Ltd., Beijing, China). Diaminobenzidine and hematoxylin were purchased from DAKO (Santa Clara, CA, USA). Hoechst 33342 and 3,3'-dioctadecyloxacarbocyanine, perchlorate (DiO) (Vybrant™ DiO Cell-Labeling Solution) were purchased from Thermo Fisher Scientific (Waltham, MA, USA).

2.2. Preparation of reduction-sensitive DOX/CS-NPs

Chitosan Lipoic acid (CSLA) NPs were prepared as previously

reported, but with some modifications [21]. Briefly, 10 mg CSO was dissolved in deionized water and stirred at room temperature. Subsequently, the solution was sonicated for 30 min (250 watts; Sonifier 250; Branson Ultrasonics, Danbury, CT, USA). Afterwards, the CSO solution was adjusted to pH 5. LA was dissolved in ethanol and added to the CSO solution. The reaction was kept at 45 °C for 12 h to synthesize CS-LA NPs. Next, CS-LA NPs were collected and purified by means of dialysis. The DOX and Cy5-loaded CS-LA NPs were synthesized using the same protocol by adding DOX and Cy5 [22]. The encapsulation efficiency (EE) and loading capacity (LC) of DOX-loaded CS-NPs were determined by SpectraMax® iD3 Multi-Mode Microplate Readers (Marshall Scientific, Hampton, NH, USA).

2.3. Characterization of DOX/CS-NPs

The size and zeta potential of DOX/CS-NPs were measured by dynamic light scattering (DLS; Zetasizer, NANO-ZS, Malvern Ltd., UK). Thereafter, the NPs were characterized by proton nuclear magnetic resonance ¹H NMR (Bruker, Bremen, Germany).

2.4. Preparation of RBCMs and 4T1CMs

To prepare RBCMs, peripheral blood of BALB/c mice was washed with 1 × PBS and centrifuged at 800 ×g to remove blood plasma. The RBC ghosts were obtained by treatment of RBCs with a hypotonic buffer (Tris, MgCl₂, K₂Cl, CaPO₄ with protease inhibitor) at 4 °C for 4 h. The RBCMs were obtained by centrifugation at 21,000 g for 30 min [24,25]. The RBCMs were further washed with deionized water, sonicated and finally stored at -80 °C until further use. In order to prepare the 4T1 CM-coated NPs, 4T1 cells were cultured in RPMI medium in T-175 cultures flasks. After the cells were grown to full confluence, they were washed with PBS and harvested using a cell scraper. The 4T1 cells were suspended in cold hypotonic buffer and further sonicated. The sample solution was centrifuged at 3200 ×g at 4 °C for 5 min. Next, the supernatants were centrifuged at 21,000 ×g for 45 min. Finally, 4T1 CMs were sonicated, dissolved in H₂O and stored at -80 °C until further use [1,26,27].

2.5. Generation and characterization of RBC-4T1 hybrid membranes, RBC-4T1@DOX/CS-NPs, RBC@DOX/CS-NPs and 4T1@DOX/CS-NPs

To obtain the RBC-4T1 hybrid membrane, RBCMs and 4T1CMs were fused using the sonication method [28]. RBC-4T1 CMs were characterized by DLS and nanoparticle tracking analysis (NTA; NanoSight® NS300, Malvern). DLS was used to determine the size and zeta potential, while NTA was used to quantify the concentration of RBCMs and 4T1 CMs. RBCMs were added to 4T1 CMs at the weight ratios of 1:1, 1:2 and 1:3. Then, they were sonicated (130 W; 42 kHz) at 37 °C for 10 min to obtain RBC-4T1 CMs [5,29,30]. The DOX/CS-NP solution in H₂O was added to a RBC-4T1 solution in PBS at the weight ratios of 1:2:1 and sonicated (130 W; 42 kHz) at 37 °C for 10 min to obtain RBC-4T1@DOX/CS-NPs. RBC@DOX/CS-NPs were also obtained and characterized by the same method at the weight ratio of 2:1 CMs to DOX/CS-NPs.

2.6. Particle surface and morphology

The morphology and shape of all NPs were imaged and analyzed by transmission electron microscopy (TEM). Briefly, before staining, carbon-coated grids (Formvar/Carbon on 200 Mesh Copper; AGS162; Van Loenen Instruments; Zaandam, the Netherlands) were glow-discharged using the Emitech K950X Turbo Evaporator (Quorum Technologies; Ashford, UK) at 2×10^{-1} mbar and 20 mA for 1 min. Next, 3 μL of sample solution were applied on the freshly glow-discharged grid and allowed to adhere for 1 min. Afterwards, excess liquid was discarded by blotting onto a filter paper and 3 μL of 2 % uranyl acetate in distilled water were

applied to the grid for negative staining of the sample. After 1 min, excess uranyl acetate was removed by blotting and the sample was air-dried for 10 min. Grids were mounted on a room temperature holder and examined using a Tecnai 12 Twin (FEI Company; Hillsboro, Oregon, USA) equipped with an OneView Camera Model 1095 (Gatan; Pleasanton, California, USA) at a voltage of 120 kV. Digital images were acquired and stored using Digital Micrograph 3.4 (Gatan).

2.7. In vitro release of DOX-loaded CSLA-NPs

The release profiles of DOX-loaded CS-NPs, RBC@DOX/CS-NPs, 4T1@DOX/CS-NPs and RBC-4T1@DOX/CS-NPs were measured by the dialysis bag diffusion method at 37 °C in different release media, including Phosphate Buffered Saline (PBS; pH 7.4), GSH (10 mM), PBS (pH 5.3), and GSH (10 mM) [21]. The dialysis tube (SERVAPOR®, MWCO 12000–14,000, Heidelberg, Germany) was used to quantify the DOX release. Afterwards, the released DOX was evaluated by SpectraMax® iD3 Multi-Mode Microplate Readers (Marshall Scientific, Hampton, NH, USA).

2.8. Membrane protein characterization

2.8.1. Sodium dodecyl sulfate polyacrylamide gel electrophoresis (SDS-PAGE)

4T1 CMs, 4T1@DOX/CS-NPs, RBCMs, RBC@DOX/CS-NPs, RBC-4T1CMs and RBC-4T1@DOX/CS-NPs with the loading buffer were heated at 95 °C for 15 min. Afterwards, 30 µL of the samples were loaded into each well of a 10 % SDS-PAGE gel and then run at 100 V for 1 h. Next, the gel was stained with Coomassie Blue for 10 min and then washed to visualize protein bands by ChemiDoc™ Touch Imaging System (Bio-Rad, the Netherlands) [31].

2.8.2. Western blotting (WB)

After electrophoresis, the protein bands were transferred onto PVDF membrane (150 V, 60 min). Then, the PVDF membrane was stained with primary antibodies followed by detection with IRDyeR680CW-labeled secondary antibody. Finally, the bands were visualized with the Li-Cor Odyssey 9120 Infrared Imaging System (Lincoln, NE, U.S.A) [32].

2.9. In vitro cellular studies

2.9.1. Cytotoxicity assays

3-(4,5-dimethylthiazol-2-yl)-5-(3-carboxymethoxyphenyl)-2-(4-sulfophenyl)-2H-tetrazolium (MTS) assay was used to determine the cellular cytotoxicity of our formulations. Briefly, 4T1 cells were seeded in 96-well plates (5.0×10^3 cells/well) and cultured at 37 °C for 24 h. Subsequently, 4T1 cells were treated with free DOX, DOX/CS-NPs, 4T1@DOX/CS-NPs, and RBC@DOX/CS-NPs for another 24 h. Afterwards, the 4T1 cells were incubated with 100 µL of fresh medium containing 20 µL MTS reagent in an incubator for 2 h. The cell viability was determined by measuring the absorbance at a wavelength of 490 nm using a SpectraMax M3 Multi-Mode Microplate Reader (Molecular Devices, Silicon Valley, CA, USA).

2.9.2. In vitro cellular uptake and distribution of DOX-loaded NPs by confocal laser scanning microscopy (CLSM)

5×10^3 cell 4T1 cells were seeded on microscope slides in a 24-well plate and were incubated for 24 h. Subsequently, the culture medium was replaced with medium containing DOX, DOX/CS-NPs, 4T1@DOX/CS-NPs and RBC@DOX/CS-NPs with the final concentration of 10 µg/mL DOX. After incubation for 3 h, the cells were washed with PBS and fixed with 4 % paraformaldehyde (PFA) for 10 min. After staining the nuclei of cells with Hoechst 33342 for 15 min, the slides were imaged by a CLSM Leica TCS SP8 (Leica Microsystems, Wetzlar, Germany).

2.9.3. Immune evasion detection

Cells of the mouse macrophage cell line RAW 264.7 were seeded in 24-well plates (1×10^4 cells/well) and cultured for 24 h. After incubation, the cells were cultured with DOX/CS-NPs, 4T1@DOX/CS-NPs, RBC@DOX/CS-NPs and RBC-4T1@DOX/CS-NPs (with the same concentration of DOX: 10 µg/mL) for 3 h and 6 h. Then, the cells were washed with PBS and stained with Hoechst 33342 for 10 min. Afterwards, the cells were imaged by CLSM and analyzed using LAS X. To study the uptake of DOX/CS-NPs, 4T1@DOX/CS-NPs, RBC@DOX/CS-NPs and RBC-4T1@DOX/CS-NPs by RAW 264.7 cells (1×10^4 cells/well) were seeded and cultured for 24 h. The day after, the cells were treated with NPs for 3 h and 6 h. Subsequently, the cells were collected for flow cytometry (BD Biosciences, Franklin Lakes, NJ, USA). experiment. The results were analyzed with the FlowJo™ v10.7.1 software (BD Biosciences).

2.9.4. Homotypic targeting study of 4T1 cells by CLSM and flow cytometry

To prove the *in vitro* homotypic targeting effects of 4T1@Cy5/CS-NPs on 4T1 qualitatively, CLSM was used to investigate the intracellular uptake of 4T1@Cy5/CS-NPs by 4T1 cells. Therefore, 1×10^4 cells (4T1, MC38, CT-26, RAW 264.7 and 3 T3) were seeded on microscope slides and incubated at 37 °C for 24 h. Then, the cells were incubated with 4T1@Cy5/CS-NPs (50 µg/ml) for 4 h. The cells were washed with PBS and fixed with 4 % PFA. This was followed by nuclear staining with Hoechst 33342 for 10 min. As a control, 4T1 cells were incubated with Cy5/CS-NPs at the same concentration for 4 h. Finally, the intracellular uptake of 4T1@Cy5/CS-NPs and Cy5/CS-NPs were analyzed by a CLSM Leica TCS SP8. The images were analyzed using LAS X (Leica Application Suite X) software. To detect the phagocytic efficiency of 4T1@Cy5/CS-NPs and DiD@PLGA-NPs (control NPs) in different cell types. Briefly, cells (4T1, MC38, CT-26, RAW 264.7 and 3 T3) were seeded into 96-well plates at a density of 1×10^4 cells/well for 24 h. Subsequently, the cells were incubated with 4T1@Cy5/CS-NPs and DiD@PLGA-NPs for 1 and 4 h. Untreated cells were used as a negative control. The cells were then washed with PBS and digested with trypsin. Later, the fluorescence intensity of 4T1 cells was detected by means of flow cytometry.

2.10. Animals

Female BALB/c mice [RRID:IMSRCRL:028] approximately 7–9 weeks old weighing between 21 and 28 g were used for the experimental orthotopic breast cancer model and toxicity studies. Animals were purchased from the Keizo Asami Immunology Laboratory (LIKA; Recife, PE, Brazil) and treated according to the ethical principles for animal experimentation. All animal procedures were approved by the Laboratory Animal Management Committee and Ethics Committee of Federal University of Rio Grande Norte (No. 063/2016). Mice were kept in an air-conditioned room at 21–22 °C, 50 % humidity, specific pathogen-free conditions, and a 12-h light/dark cycle. A group of five mice were housed in a cage. They had free access to food and water and were randomly grouped ($n = 6$) and kept in different cages. After 1 week and adaption of the mice to the environment, the animal experiment was commenced.

2.10.1. In vivo antitumor activity

In this experiment, 4T1 cells (1×10^6 cells/100 µL FBS-free DMEM) were inoculated below the fourth left breast in BALB/c mice anesthetized with xylazine and ketamine (2:8). Then, the mice were randomized into 6 groups with $n = 6$ animals each. Tumor growth was monitored every two days. When the tumors reached 3 mm in diameter, the mice were treated peritumorally with sterile saline (negative control group), DOX (0.125 mg/Kg; positive control), DOX/CS-NPs (0.125 mg/Kg), RBC@DOX/CS-NPs (0.125 mg/Kg), 4T1@DOX/CS-NPs (0.125 mg/Kg) and RBC-4T1@DOX/CS-NPs (0.125 mg/Kg). Every 5 days, treatments were repeated for a total of 3 times over 15 days. The animals were anesthetized and killed by cervical dislocation on day 19.

Subsequently, blood (from the heart cavity), tumor, lungs and liver were collected for biochemical and histopathological analysis.

2.10.2. Biochemical and hematological analysis

After storage, standard hematological techniques were performed on EDTA-treated blood. Thus, erythrocyte and leukocyte count as well as hemoglobin quantification and hematocrit test were carried out. The blood of all animals in each group ($n = 6$) was analyzed in triplicate.

2.10.3. qRT-PCR

Partial orthotopic tumors from BALB/c mice were analyzed to ascertain the gene expression. The total RNA orthotopic tumor was obtained with Invitrogen™ TRIZol™ reagent (Fisher Scientific, USA) and purified with SV Total RNA Isolation System (Promega, USA) according to the manufacturer's instructions. Next, cDNA was synthesized using high-capacity RNA-to-cDNA™ kit (Applied Biosystems, USA). PowerUp SYBR Green Master Mix (Applied Biosystems, USA) was used for real-time amplification. In the (Supplementary Table 1), the forward and reverse primers sequences (Thermo Fisher Scientific, USA) are listed. The experiments were performed in triplicate. Gene expression data were normalized relative to the housekeeping gene β -actin using $2^{-\Delta\Delta Ct}$. All animals in each group ($n = 6$) were analyzed in duplicate.

2.10.4. Histology and immunohistochemistry

For immunohistochemical analysis, the tumors and organs of BALB/c mice were collected. Briefly, after deparaffinization, rehydration and antigen recovery, the tumor tissue sections were incubated with anti-NF- κ B, anti-CD163 and anti-CXCL12 at 4 °C overnight. As a secondary antibody, biotinylated pan-specific universal antibody was used followed by incubation with HRP-conjugated streptavidin. Next, diaminobenzidine (DAB; DAKO) was used to reveal the labeling. Sections were counterstained with hematoxylin and analyzed under a Nikon E200 LED light microscope (Minato, Japan). According to Charafe-Jauffret [33] for immunoreactivity classification, the percentage of positively stained cells and intensity of positive cells after immunostaining was calculated. Immunohistochemical analyses of tumor tissues were performed independently by two trained researchers. Blind data analysis was applied for the scoring of the tumor tissues. For each antibody, three histological sections were evaluated.

2.11. Statistical analysis

Analyses were performed using GraphPad Prism 8.1.1 software (GraphPad Software, San Diego, CA, USA). All data are presented as mean \pm standard deviation (SD). All data were statistically analyzed using student's *t*-test, analysis of variance (ANOVA; nonparametric) with Bonferroni test, unpaired and Mann-Whitney *U* test. Significance levels were defined as # (not significant, $P \geq 0.05$), * $P \leq 0.05$, ** $P \leq 0.01$, *** $P \leq 0.001$ and **** $P \leq 0.0001$.

3. Results

3.1. Preparation and characterization of DOX/CS-NPs, 4T1@DOX/CS-NPs, RBC@DOX/CS-NPs and RBC-4T1@DOX/CS-NPs

DOX/CS-NPs were synthesized as reduction-sensitive NPs for the treatment of 4T1 tumors. Various reduction-sensitive polymeric NPs for targeted therapy of breast cancer, including the triple-negative breast cancer cell line 4T1, have been reported [34]. To prepare the 4T1CM and RBCM-coated DOX/CS-NPs, 4T1CMs and RBCMs were isolated using hypotonic lysis buffer and differential ultracentrifugation. RBCMs and 4T1CMs were mixed for the generation of fusion membranes at a ratio of 1:1, 1:2 and 1:3 and were quantified by NTA (Fig. S1) [5]. To further confirm the successful fusion of 4T1CMs and RBCMs, we labeled 4T1CMs with DiD (purple; $\lambda_{ex}/\lambda_{em} = 646/663$ nm) and RBCMs with DiO (green; $\lambda_{ex}/\lambda_{em} = 484/501$ nm). A diluted sample of RBCMs and

4T1CMs was prepared and imaged by CLSM and confirmed successful fusion (Fig. 1A). Our data confirmed the successful fusion of RBC-4T1 membranes, and established that the ratio of 1:2 was optimal. Next, 4T1CMs, RBCMs and RBC-4T1CMs were coated onto DOX/CS-NPs at a ratio of 2:1, 2:1 and fusion membranes at ratio of 1:1:1, 1:2:1 and 1:3:1 (Fig. 1B). The size of RBC-4T1 fusion membranes at a ratio of 1:3 was bigger than at a ratio of 1:2 and 1:1. In addition, at a ratio of 1:1, the positive surface charge of DOX/CS-NPs was not sufficiently decreased (Fig. S 2), suggesting incomplete coating of DOX/CS-NPs. TEM images revealed that CM-coated DOX/CS-NPs were of spherical shape, which were composed of DOX/CS-NPs as inner core and 4T1CMs, RBCMs and RBC-4T1CMs as the shell (Fig. 1C). In addition, the NPs were characterized by DLS measurements. The DOX/CS-NPs showed an average hydrodynamic diameter of 278 ± 1.62 nm, polydispersity index (PDI) of 0.352 ± 0.092 and a surface charge of $+44 \pm 0.15$ mV (Fig. 1D,E). Successful surface coating of DOX/CS-NPs with 4T1CMs and RBCMs was additionally confirmed by an increase in particle size and a reduction in NP surface charge of 4T1CM-, RBCM- and 4T1-RBCM-coated DOX/CS-NPs, as measured by DLS (Fig. 1D, E). To this end, for coating of DOX/CS-NPs with RBC-4T1CMs optimized ratio was obtained at 1:2:1, indicating suitable size of NPs and sufficient coating (Fig. 1B).

The successful conjugation of LA to CSO was investigated by 1 H NMR (Fig. 2A). As reported in our previous study, the determined proton peaks of penta-heterocyclic structure of LA at 2.5–3.5 ppm in CS-LA NPs are a proof of LA conjunction [21]. The EE% and LD% of DOX in CS-NPs were calculated to be 71.76 ± 0.87 and 38.03 ± 0.45 , respectively. The release of DOX from DOX/CS-NPs, RBC@DOX/CS-NPs, 4T1@DOX/CS-NPs and RBC-4T1@DOX/CS-NPs was studied at 37 °C in pH 7.4 and pH 5.3, with and without addition of 10 mM GSH (Fig. 2B-E). The results showed that the addition of 10 mM GSH significantly induced (**** $p \leq 0.0001$) the release of DOX from DOX/CS-NPs (Fig. 2B-E) [21,22]. In addition, an acidic milieu (pH 5.3) significantly (**** $p \leq 0.0001$) increased the release of DOX from DOX/CS-NPs (approximately 82 %,) after 24 h, compared to pH 7.4 (44 %). However, RBC@DOX/CS-NPs and 4T1@DOX/CS-NPs as well as RBC-4T1@DOX/CS-NPs sustained DOX release profile in pH 7.4 and pH 5.3, with and without 10 mM GSH (Fig. 2C, E) indicating the efficiency of exciting coating and stability of membrane-coated NPs during the physiological states [3,35]. The successful transfer of membrane proteins is important for the exploitation of CMs for tumor targeting. In order to determine the membrane proteins of 4T1CM-coated DOX/CS-NPs, we employed SDS-PAGE and WB (Fig. 2D, E). SDS-PAGE of cell lysates of 4T1 cell, 4T1CM, 4T1@DOX/CS-NPs, RBCMs, RBC@DOX/CS-NPs, RBC-4T1CMs and RBC-4T1@DOX/CS-NPs demonstrated the successful transfer of proteins from 4T1CMs, RBCMs and RBC-4T1CMs onto the outer layer of DOX/CS-NPs (Fig. 2D, E). Next, we investigated the successful transfer of CM by WB labeling for the membrane protein CD47, which is expressed by 4T1 tumor cells and is relevant for homotypic targeting and reduction of uptake by macrophages [1,14,36]. Our results showed that CD47 was present in the lysates of 4T1 cells, 4T1CMs and 4T1@DOX/CS-NPs, confirming the successful coating of DOX/CS-NPs with 4T1CMs.

3.2. Effective internalization and enhanced cytotoxicity of DOX/CS-NPs coated with 4T1CMs by 4T1 breast cancer cells

The cellular uptake of free DOX, DOX/CS-NPs, 4T1@DOX/CS-NPs, RBC@DOX/CS-NPs and RBC-4T1@DOX/CS-NPs was determined by CLSM and flow cytometry. 4T1 cells were incubated with our NP formulations for 4 h. Cellular NP uptake depends on many factors including NP size, PDI, surface charge and surface modification [9]. CLSM data showed that the positively charged RBC@DOX/CS-NPs and 4T1@DOX/CS-NPs, as well as the negatively charged RBC-4T1@DOX/CS-NPs exhibited higher uptake by 4T1 cells compared to DOX/CS-NPs and free DOX (* $p \leq 0.05$, *** $p \leq 0.0001$), and therefore improved cellular uptake of DOX by NPs (Fig. 3A, B). Previous reports showed that free DOX diffused to the nuclei 2 to 8 h after uptake [37]. CLSM analysis

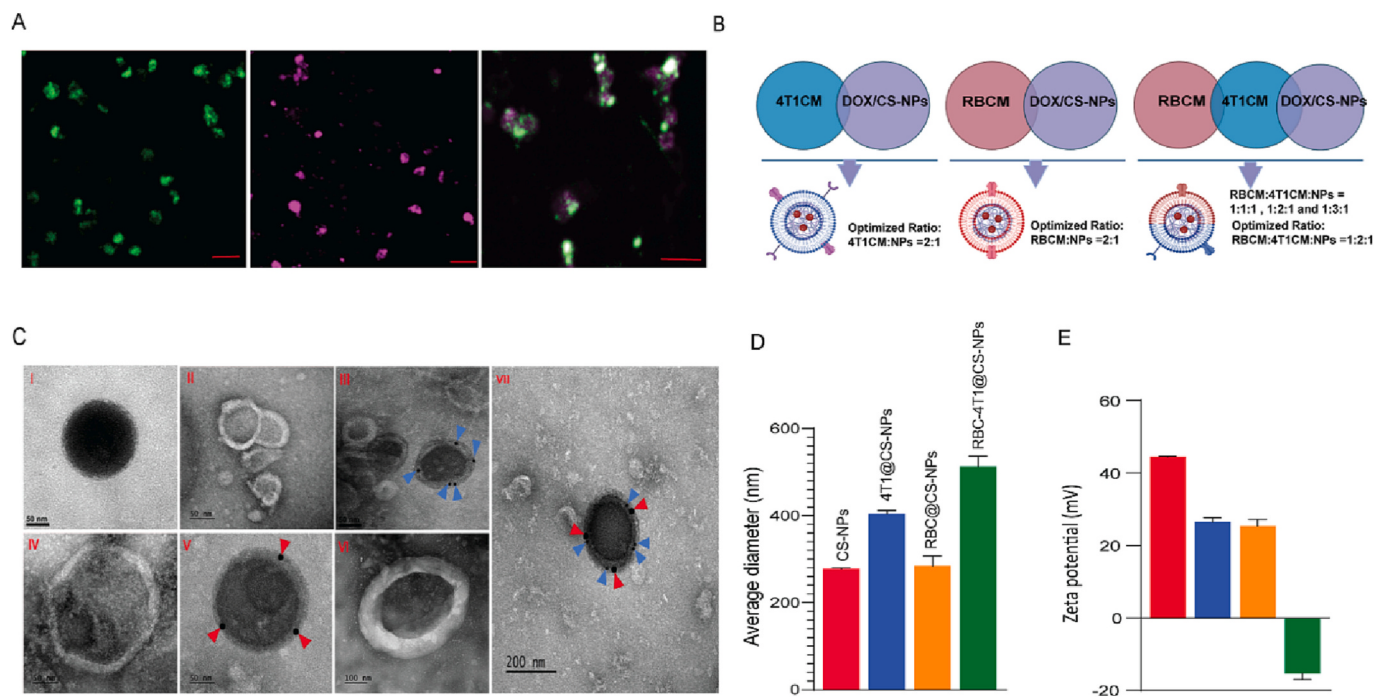


Fig. 1. Characterization of different NP formulations. A) CLSM images of DiD-labeled 4T1CMs (purple), RBCMs-labeled DiO (green), and the merged images of 4T1CMs and RBCMs (scale bar = 5 μ m). B) Schematic illustration showing the overview of the combinations of the 4T1CMs, RBCMs and DOX/CS-NPs used for designing DOX/CS-NPs, 4T1@DOX/CS-NPs, RBC@DOX/CS-NPs and RBC-4T1@DOX/CS-NPs. C) TEM images of I) DOX/CS-NPs, II) 4T1CMs, III) 4T1@DOX/CS-NPs, IV) RBCMs, V) RBC@DOX/CS-NPs, VI) RBC-4T1 CMs and VII) RBC-4T1@DOX/CS-NPs. D, E) Particle size and zeta potential of DOX/CS-NPs, 4T1@DOX/CS-NPs, RBC@DOX/CS-NPs and RBC-4T1@DOX/CS-NPs by DLS.

revealed that, while free DOX localized to the nucleus 4 h after incubation, the majority of NP-encapsulated DOX localized to the cytosol, in line with our release kinetics data showing that only a fraction of DOX was released at this timepoint (Fig. 2B). Both CLSM and flow cytometry data showed that uptake of NP-encapsulated DOX was overall higher than uptake of free DOX (Fig. 3A,B). Flow cytometric analysis further revealed that between the targeted NPs, uptake of 4T1@DOX/CS-NPs was highest (Fig. 3B). This increased uptake of 4T1CMs can be attributed to the transfer of targeting proteins present on 4T1CMs, which mediate homotypic targeting towards source cells. Cell viability assays of 4T1 cells incubated with free DOX and DOX/CS-NPs revealed an IC₅₀ of 0.85 and 0.91 μ g mL⁻¹, respectively (Fig. 3C). However, when DOX/CS-NPs were coated with 4T1CMs (4T1@DOX/CS-NPs), they displayed an IC₅₀ of 0.59 μ g mL⁻¹, which is 1.5-fold lower than that of non-targeted NPs (control). Thus, 4T1CM-coating led to higher cytotoxicity likely as a result of increased cellular internalization of 4T1@DOX/CS-NPs by 4T1 cells, compared to DOX/CS-NPs (Fig. 3C). Compared to 4T1@DOX/CS-NPs and DOX/CS-NPs, RBC@DOX/CS-NPs did not significantly increase cellular uptake or reduced the IC₅₀ (Fig. 3C, D) [38]. The cytotoxicity of NPs without DOX, CS-NPs, 4T1@CS-NPs, RBC@CS-NPs and RBC-4T1@CS-NPs, was studied in 4T1 and 3 T3 cells. None of the control NPs exhibited any significant cytotoxicity (Fig. 3E, F), showing that CS-NPs possess good biocompatibility.

3.3. Inhibition of macrophage-mediated NP uptake by CM-coating

Next, we studied the immune escape mechanism of DOX/CS-NPs, 4T1@DOX/CS-NPs, RBC@DOX/CS-NPs and RBC-4T1@DOX/CS-NPs. Macrophages are responsible for the *in vivo* immune clearance of NPs [39]. To investigate whether our NP formulations could escape macrophage-based clearance, we cultured the macrophage RAW 264.7 cell line with DOX-loaded CS-NPs. Then, the cells were imaged by CLSM after 3 and 6 h of incubation. The fluorescence images showed that RAW 264.7 cells incubated with DOX/CS-NPs had a the intensity of the red

fluorescence was significantly higher than that of RAW 264.7 cells incubated with CM-coated DOX/CS-NPs at 3 h and 6 h (Fig. 4A, B). The intensity of 4T1CM, RBCM and RBC-4T1CM-coated DOX/CS-NPs was lower, thereby suggesting that 4T1CM, RBC and RBC-4T1CM representing the shell of DOX/CS-NPs reduced the cellular uptake of DOX/CS-NPs. To quantify the uptake data, flow cytometric analysis was performed (Fig. 4B). The intensity of the red fluorescence of DOX/CS-NPs was about 1.3-, 1.3- and 1.2-fold higher than that of 4T1@DOX/CS-NPs, RBC@DOX/CS-NPs and RBC-4T1@DOX/CS-NPs groups, respectively (** $p \leq 0.01$, *** $p \leq 0.001$, **** $p \leq 0.0001$). The data indicate that the presence of CD47 on CM-coated DOX/CS-NPs could suppress the uptake of NPs by macrophages, which is in line with the literature [4,40,41].

3.4. 4T1 cancer cell self-recognition by homotypic targeting

To investigate the homotypic targeting capacity of CM-coated Cy5@DOX/CS-NPs (Table S2), DiD/PLGA-NPs (control NPs, Table S2), we incubated NP formulations with breast cancer cell line (4T1 cells) and the colorectal tumor cell lines (MC38 and CT-26 cells), as well as with non-tumorigenic cell lines (3 T3 and RAW 264.7 cells) (Fig. 5A-C and Fig. S3), and analyzed the cellular uptake by CLSM and flow cytometry. To this end, we used NPs encapsulated with the fluorescent dye Cy5. Both MC38 and 4T1 cells were treated with 4T1@Cy5/CS-NPs, MC38@Cy5/CS-NPs, CT26@Cy5/CS-NPs, RAW@Cy5/CS-NPs and 3 T3@Cy5/CS-NPs. Flow cytometric analysis showed a higher Cy5 signal in 4T1 cells treated with 4T1@Cy5/CS-NPs compared to the CM-coated-Cy5/CS-NPs derived from MC38, CT-26, RAW and 3 T3 cells. The fluorescence intensity in the 4T1@Cy5/CS-NPs group was about 2.7-, 1.3-, 2.1-, 1.6- and 1.8-fold higher than in 4T1 cells treated with Cy5@CS-NPs, MC38@Cy5/CS-NPs, CT26@Cy5/CS-NPs, RAW@Cy5/CS-NPs and 3 T3@Cy5/CS-NPs, respectively. To confirm our flow cytometry data, we incubated both MC38 and 4T1 cells with MC38@Cy5/CS-NPs, CT26@Cy5/CS-NPs, RAW@Cy5/CS-NPs and 3

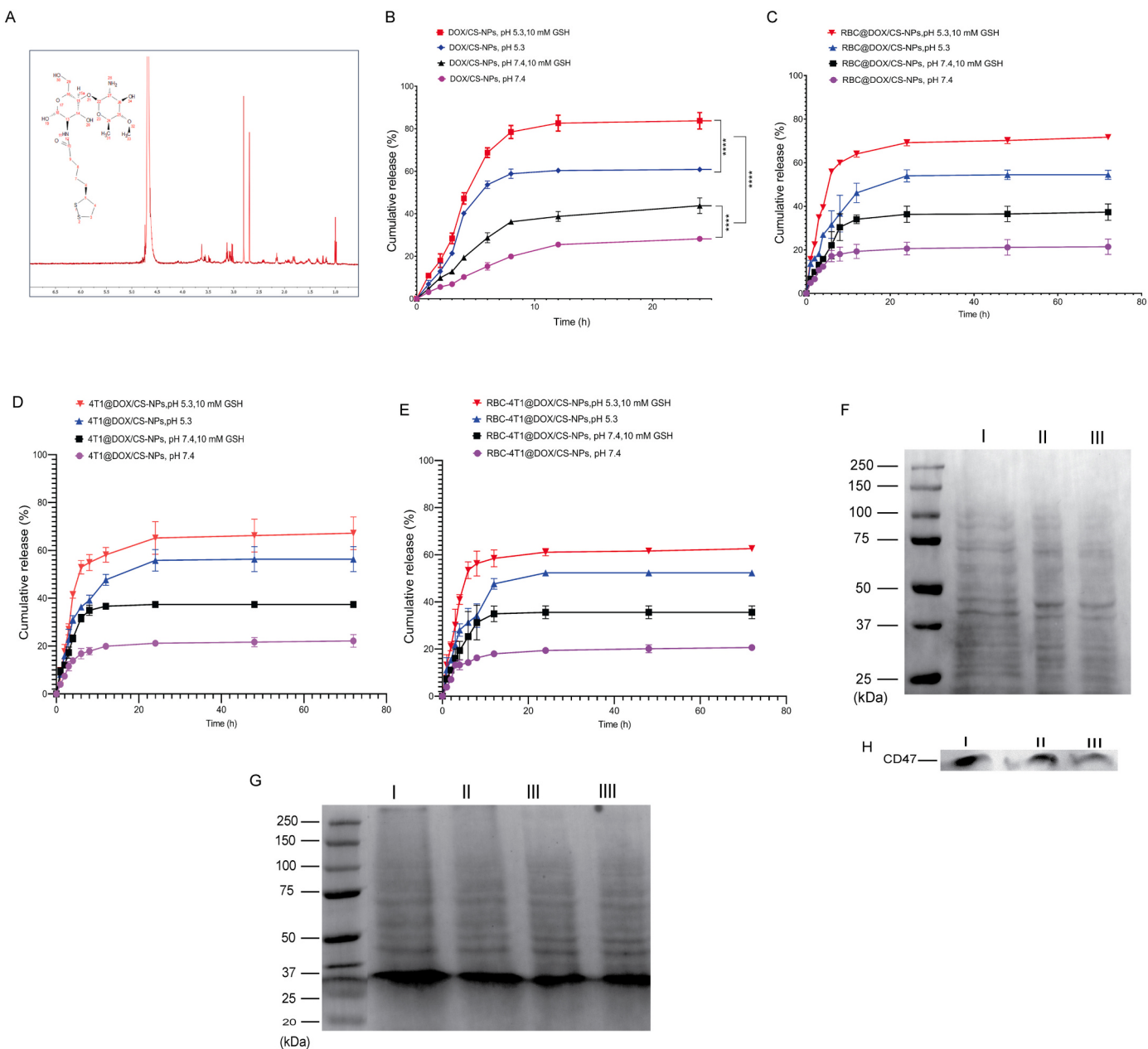


Fig. 2. A) ¹H NMR spectrum of DOX/CSLA-NPs in D₂O. B, C, D,E) *In vitro* DOX release profile of DOX/CS-NPs, RBC@DOX/CS-NPs, 4T1@DOX/CS-NPs and RBC-4T1@DOX/CS-NPs at pH 7.4 and pH 5.3, in the presence and absence of 10 mM GSH. F) SDS-PAGE and WB analysis of I) 4T1cell lysates, II) 4T1CMs and III) 4T1@DOX/CS-NPs. G) SDS-PAGE of I) RBCM, II) RBC@DOX/CS-NPs, III) RBC-4T1CM and IIII) RBC-4T1@DOX/CS-NPs. H) Western blot analysis of 4T1 cell, 4T1CM, and 4T1@DOX/CS-NPs for characteristic 4T1CM markers CD47. Data are represented as mean ± SD; ** p ≤ 0.01, *** p ≤ 0.001, **** p ≤ 0.0001.

T3@Cy5/CS-NPs for 4 h to analyze the uptake using CLSM. The images showed that the fluorescence signal of 4T1@Cy5/CS-NPs (purple) was higher than in the other samples (Fig. 5 A, B; # = not significant, P > 0.05, **P < 0.01, ***P < 0.001, and ****P < 0.0001). In addition, uptake data of control NPs (DiD@PLGA-NPs) (Fig. S3) demonstrated the ability of DiD@PLGA-NPs for homotypic targeting. Together, these results showed that the self-recognition capability of membrane-coated NPs for homotypic targeting [29,42].

3.5. Anti-tumor effect of NPs *in vivo*

The 4T1 orthotopic mammary tumor metastasis model was used to verify the *in vivo* anti-tumor effects of all our NP formulations. To this end, mice were inoculated with 1 × 10⁶ 4T1 cells on day 1. When the tumors reached a size of 3 mm in diameter, the mice were injected

intratumorally with saline, free DOX, DOX/CS-NPs, 4T1@DOX/CS-NPs, RBC@DOX/CS-NPs or RBC-4T1@DOX/CS-NPs at a dose of 0.125 mg/kg⁻¹ (n = 6; Fig. 6A). The tumor growth was monitored over the course of 19 days (Fig. 6B, C). The tumors of the saline group showed a rapid growth (Fig. 6B-C). All DOX-loaded CS-NPs coated with either 4T1CMs or RBCMs, as well as free DOX and DOX/CS-NPs, significantly inhibited the tumor growth, compared to the saline group (**P < 0.001; Fig. 6B). Interestingly, we observed a complete tumor regression in one mouse of the group treated with 4T1@DOX/CS-NPs (Fig. 6A). After coating the DOX/CS-NPs with 4TCMs and RBCMs, the tumor growth was dramatically reduced by 95 % and 90 %, respectively, compared to the saline group (**P < 0.001; Fig. 6C). As shown in Fig. 6D, tumor weight was significantly reduced in the groups treated with free DOX, DOX/CS-NPs, 4T1@DOX/CS-NPs, RBC@DOX/CS-NPs and RBC-4T1@DOX/CS-NPs, compared to the saline control group. The tumor weight curves

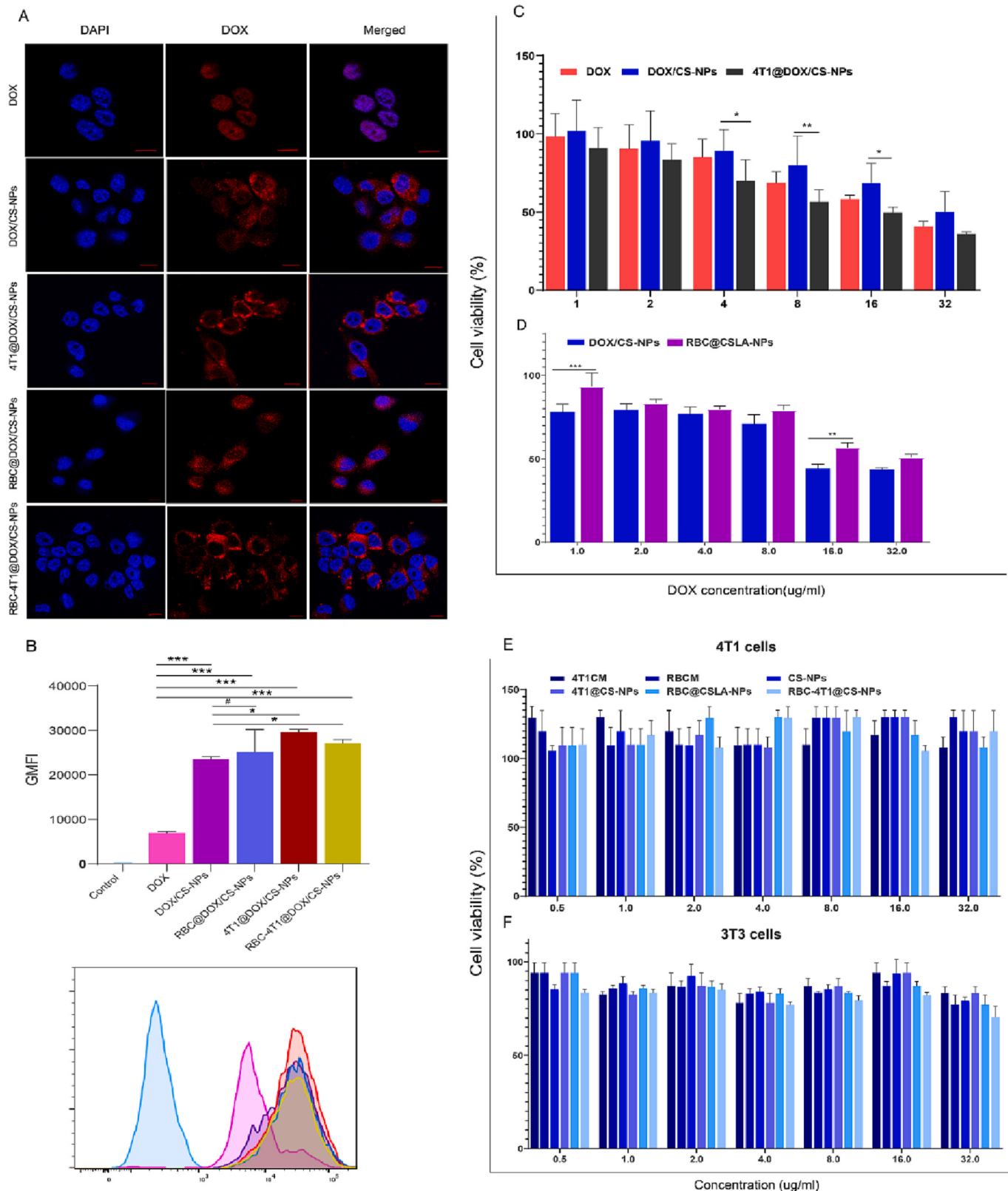


Fig. 3. Internalization and cytotoxicity of the NPs formulations. A, B) Cellular uptake of 4T1 cells with different samples after 4 h of incubation. DOX (red) and nuclei (blue) by means of CLSM and flow cytometry (scale bar = 10 μ m). C, D) *In vitro* cytotoxicity of DOX, DOX/CS-NPs, 4T1@DOX/CS-NPs and RBC@DOX/CS-NPs on 4T1 cells after 24 h. Data are represented as mean \pm SD ($n = 3$). E, F) *In vitro* cell viability of 4T1 cells and 3 T3 cells, respectively, after 24 h of incubation of 4T1CMs, RBCMs, without DOX CS-NPs, 4T1@ CS-NPs, RBC@ CS NPs and RBC-4T1@ CS-NPs. Data are represented as mean \pm SD; ** $p \leq 0.01$, *** $p \leq 0.001$, **** $p \leq 0.0001$.

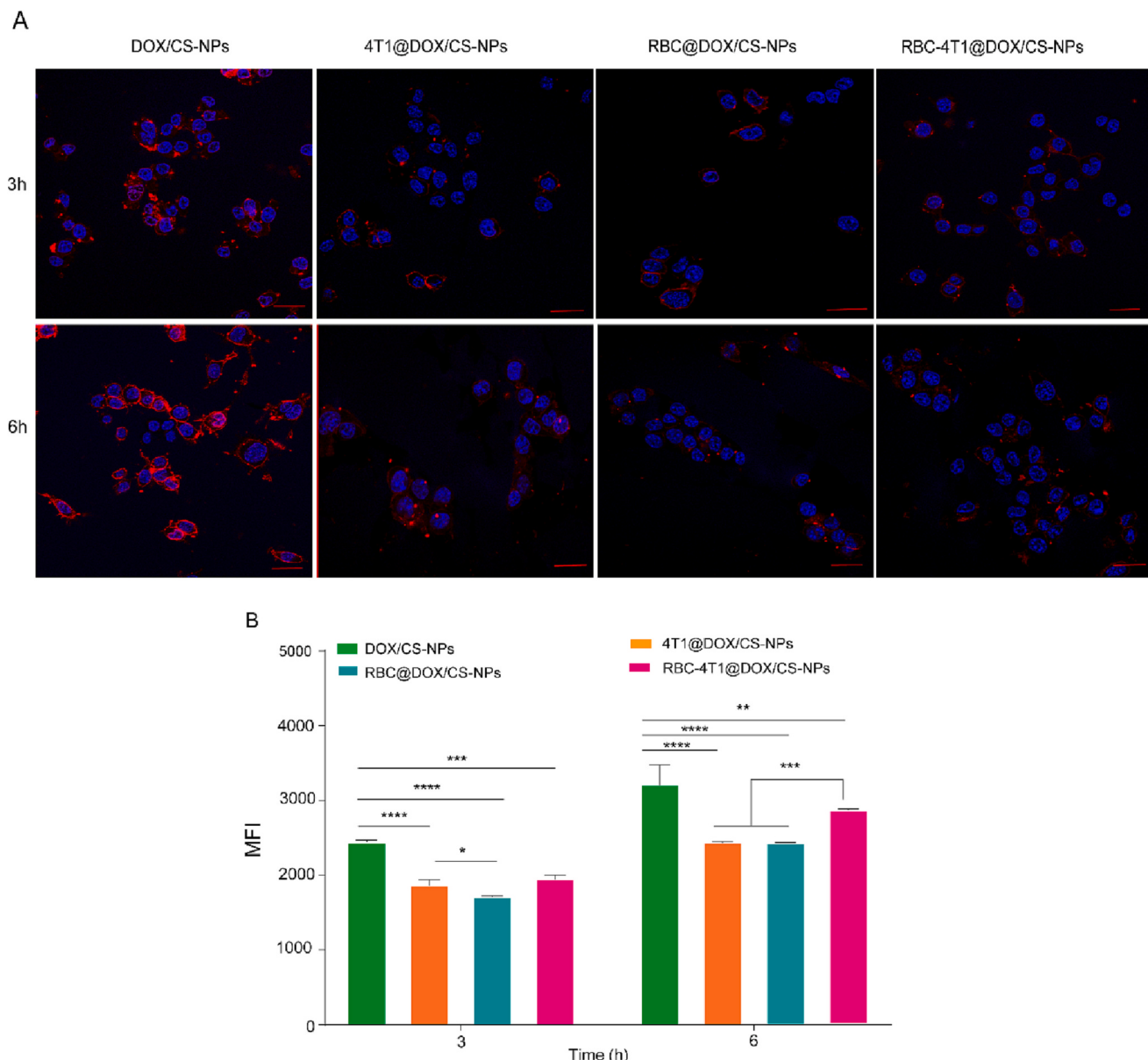


Fig. 4. Cellular uptake of different NP formulations. A) Intracellular uptake of DOX/CS-NPs, 4T1@DOX/CS-NPs, RBC@DOX/CS-NPs and RBC-4T1@DOX/CS-NPs in RAW 264.7 cells after 3 and 6 h of incubation (scale bar = 20 μ m). The nucleus was stained with Hoechst 33342 (blue) and the NPs were labeled with DOX (red). B) Intracellular fluorescence intensity of DOX measured by means of flow cytometry after 3 and 6 h of incubation. Data are represented as mean \pm SD ($n = 3$); ** $p \leq 0.01$, *** $p \leq 0.001$, **** $p \leq 0.0001$.

illustrated that DOX/CS-NPs coated with RBC and 4T1CMs had a similar effect on reducing tumor weight. Free DOX reduced the tumor weight to 120 mg, while tumor weight of the groups treated with saline, DOX/CS-NPs and RBC-4T1@DOX/CS-NPs were 305.5 mg, 130.75 mg and 127.1 mg, respectively. In the groups treated with RBC@DOX/CS-NPs and 4T1@DOX/CS-NPs, the tumor weight was reduced to 41.16 mg and 16.9 mg, respectively. The data of the tumor volume at endpoint similarly illustrated a significant reduction in tumor volume in the groups treated with DOX, DOX/CS-NPs, 4T1@DOX/CS-NPs, RBC@DOX/CS-NPs and RBC-4T1@DOX/CS-NPs, compared to the saline group (Fig. 6C). The results suggest that 4T1CM-coated NPs induced homotypic targeting, which enhanced the uptake efficiency of 4T1@DOX/CS-NPs in 4T1 source cells *in vivo* and improved DOX accumulation [14]. In addition, due to the RBCM coating, RBC@DOX/CS-NPs were less likely to be cleared by the immune system than uncoated NPs [43]. The blood leukocyte count of the mice after treatment with NPs was measured to show whether the treatment had any deleterious effect on the immune

system (Fig. 6E). The data illustrated that the leukocyte counts in the groups treated with DOX were significantly lower than those treated with the saline. However, the reduction in leukocyte counts in the 4T1@DOX/CS-NP-treated group was less compared to DOX treatment.

3.6. Inhibition of breast cancer metastasis by NPs

4T1 cells have been shown to rapidly divide and spontaneously metastasize [44]; they can spread into the liver, lungs and lymph nodes [45]. In this study, after treatment of mice with DOX-loaded CS-NPs, the presence of infiltrating tumor cells was histologically analyzed in the liver and lungs of 4T1 tumor-bearing mice (Fig. 7A, B, arrowheads). Scoring of infiltrating tumor cells revealed that in all experimental groups, tumor cells infiltrated the liver, except for groups treated with CS-NPs- and RBC-4T1@DOX/CS-NPs. However, compared to the saline group, the number of metastatic niches was reduced in mice treated with DOX, 4T1@DOX/CS-NPs and RBC@DOX/CS-NPs (* $P < 0.05$, ** $P <$

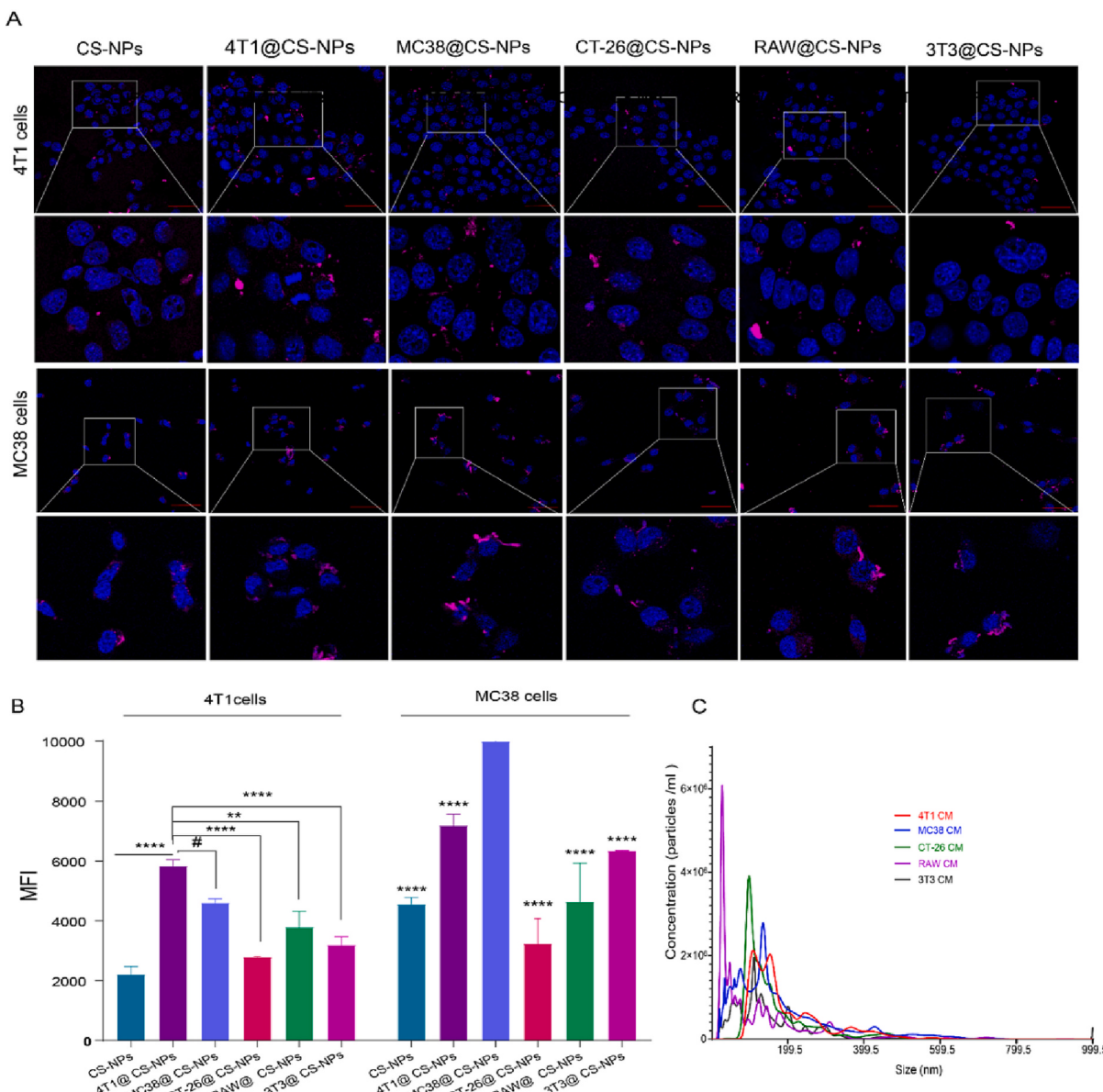


Fig. 5. Cellular uptake of different NP formulations. A) CLSM images and B) flow cytometric profiles of 4T1 and MC38 cells after 4 h of incubation with Cy5-loaded CS-NPs coated with CMs derived from five different cell lines, i.e. 4T1@CS-NPs, MC38@CS-NPs, CT-26@CS-NPs, RAW@CS-NPs and 3 T3@CS-NPs (scale bar = 50 μm). C) NTA analysis of 4T1, MC38, CT-26, RAW 264.7 and 3 T3 CMs. Data are represented as mean ± SD; # $P \geq 0.05$, * $P \leq 0.05$, ** $P \leq 0.01$, *** $P \leq 0.001$ and **** $P \leq 0.0001$.

0.01, and **** $P < 0.0001$; Fig. 7A, C). In addition, we analyzed the number of niches in the lung tissue for all treatment groups and observed no metastatic niches, except for mice treated with saline and RBC@DOX/CS-NPs (**** $P < 0.0001$; Fig. 7B, C). Our data demonstrate that lung and liver metastasis was significantly decreased in all treatment groups in tumor-bearing mice, compared to the saline-treated control group.

3.7. Gene and protein expression profile in tumor microenvironment

We carried out immunohistochemistry (IHC) and RT-qPCR analysis of sections of 4T1 breast tumors to analyze different oncological parameters, including cell survival, immune regulation and drug resistance. As shown in Fig. 8A, B, the expression of *NfkB1*, which promotes angiogenesis and cancer invasion was significantly downregulated after treatment with free DOX, 4T1@DOX/CS-NPs and RBC-4T1@DOX/CS-NPs (** $p \leq 0.001$, **** $p \leq 0.0001$). Previous studies showed that

CXCL12 plays a role in the development of metastasis and invasion of breast cancer [46]. Analysis of CXCL12 protein expression showed that all treatments significantly downregulated CXCL12 in the TME (**** $p \leq 0.0001$). Interestingly, the downregulation of CXCL12 in the group treated with 4T1@DOX/CS-NPs (H-score: 12.67 ± 2.5) was 8.8-fold higher (**** $p \leq 0.0001$) than in the free DOX group (H-score: 112.5 ± 7.5) and 1.20-fold higher than in the group treated with DOX/CS-NPs (H-score: 15 ± 2 ; Fig. 8C). In addition, the immunomodulatory effect of the NPs on the TME was studied by IHC. The data indicated that the expression of the M2 tumor-associated macrophage (TAM) marker CD163 was downregulated in all treatment groups. However, the downregulation effect was most prominent in the mice treated with 4T1@DOX/CS-NPs (Fig. 8D).

Two important hallmarks of cancer were evaluated through genetic expression: signaling pathways of i) apoptosis (FAAD and APAF-1) and ii) immunosuppression (CD163 and CD8). The RT-qPCR data showed that the treatment of tumor-bearing mice with free DOX, DOX/CS-NPs,

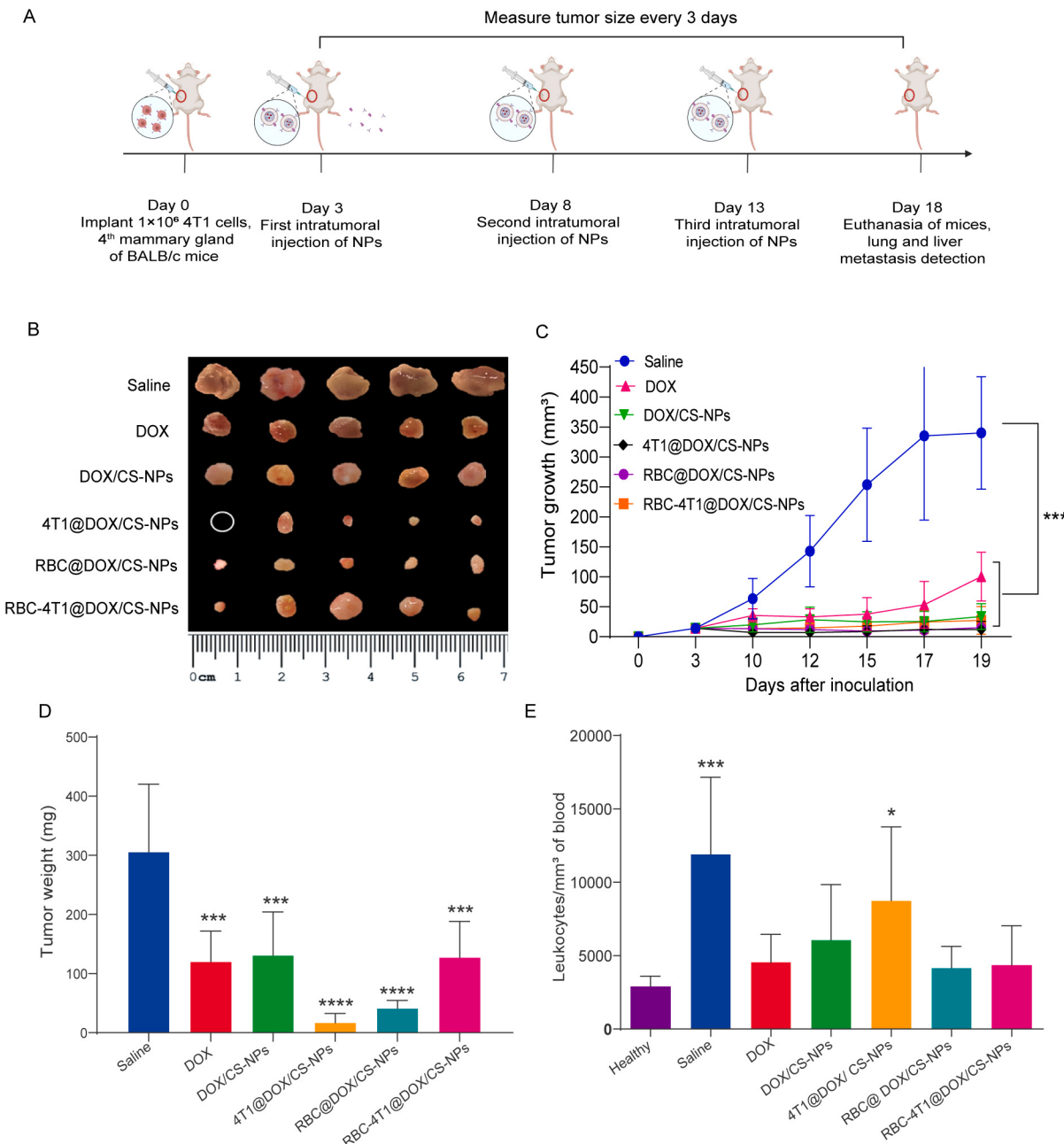


Fig. 6. *In vivo* experiments in BALB/c mice bearing 4T1 breast tumors. A) Experimental timeline: 1×10^6 4T1 cancer cells were implanted at the mammary site (day 0) and mice were treated with saline, free DOX, DOX/CS-NPs, 4T1@DOX/CS-NPs, RBC@DOX/CS-NPs and RBC-4T1@DOX/CS-NPs by peritumoral injection of NPs (5 mice per group) on day 3, 8, and 13. B) Photographs of tumors taken from mice carrying 4T1 tumors at endpoint (day 18). C) Growth curves of *in situ* mammary tumors in BALB/c mice showing reduction in tumor volume after treatment with free DOX, DOX/CS-NPs, 4T1@DOX/CS-NPs, RBC@DOX/CS-NPs and RBC-4T1@DOX/CS-NPs. D) Mean weight of tumors at endpoint ($n = 5$). E) Blood leukocytes counts of mice treated with different NP formulations. Data represent mean \pm SEM; ** $p \leq 0.01$, *** $p \leq 0.001$, **** $p \leq 0.0001$ by Student's *t*-test.

RBC@DOX/CS-NPs and RBC-4T1@DOX/CS-NPs significantly upregulated the expression of the apoptotic gene *Fadd* (** $p < 0.01$, **** $p \leq 0.0001$; Fig. 9A). In addition, the expression of *Apaf-1* was upregulated in all treatment groups except for the free DOX group (Fig. 9B). Interestingly, the expression of *Birc5* (Survivin), which is an inhibitor of apoptosis [47], was significantly reduced in the mice treated with DOX/CS-NPs, 4T1@DOX/CS-NP and RBC-4T1@DOX/CS-NPs (** $p < 0.01$; Fig. 9C). The immunomodulatory effect of the NP formulations was determined by analyzing the expression of the *Cd163*, *Cd68* and *Cd8* genes in the TME. Our data indicated that 4T1@DOX/CS-NPs significantly (* $p < 0.05$, ** $p < 0.01$) reduced the expression of *Cd163*, and increased the expression of *Cd8* and *CD68* (Fig. 9E-F), suggesting

modulation of the TME towards a more pro-tumorigenic state and infiltration of CD8 lymphocytes.

4. Discussion

Recently, CM-coated NPs have been developed to increase the efficacy of drug delivery systems [48]. CM-coated NPs preserve the antigens and structure of the natural CM, thus resulting in the transfer of biological membrane properties [49]. In particular, the unique properties of biomimetic NPs include immune escape, special molecular recognition, cellular targeting and prolonged circulation time, which make them an attractive delivery system for biomedical applications [50]. To

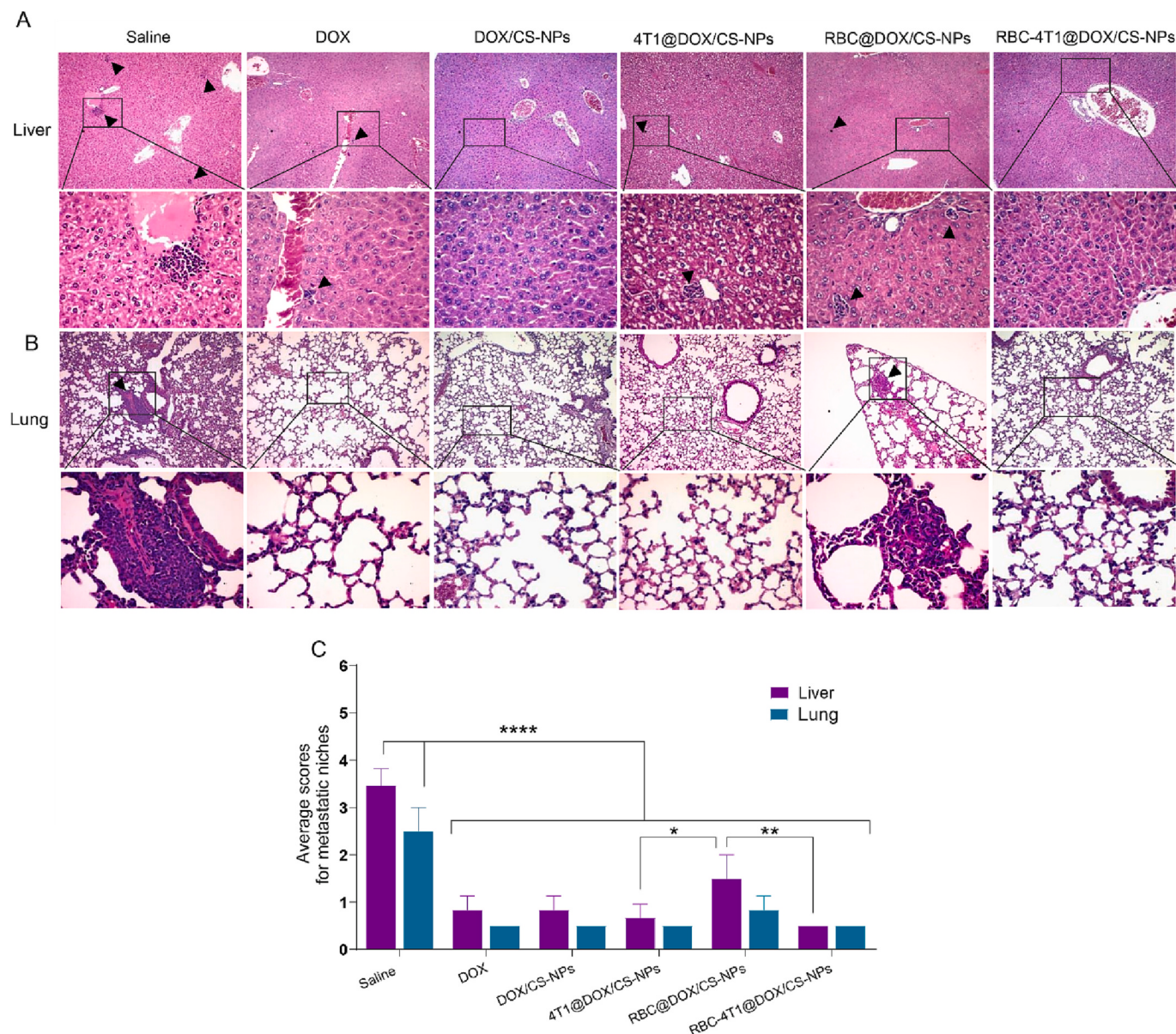


Fig. 7. Evaluation of metastatic niches. The evaluation of tumor cell migration to secondary sites observed in the (A) liver and (B) lungs. A) The arrowheads indicate the presence of metastatic. C) Metastatic niches in the liver and lungs were semi-quantitatively scored according to the percentage of tumor cells in the tissue parenchyma. * $p < 0.05$; ** $p < 0.01$, *** $p \leq 0.0001$ scale bars of $100\times = 100 \mu\text{m}$, scale bars of $400\times = 25 \mu\text{m}$.

incorporate these properties onto our NPs, we produced biomimetic NPs by using RBCMs and 4T1CMs as a shell. For effective DOX release in 4T1 cells, we formulated DOX-loaded, reduction-sensitive CSLA-NPs as a core. Our data suggest that RBCMs and 4T1CMs represent effective targeting moieties when used alone to treat 4T1 breast cancer in agreement with previous studies [24,51,52], while fusion hybrid CMs did not show beneficial targeting properties. This discrepancy could be due to an increase in size of the resulting hybrid RBC-4T1@DOX/CS-NPs, compared to RBC@DOX/CS-NPs and 4T1@DOX/CS-NPs, as a result of hybrid CM-coated NPs simultaneously carrying two membranes. For instance,

Xu et al. designed 4T1 CM-coated redox/pH dual-responsive NPs for 4T1 tumor chemotherapy [52]. They were able to show that intravenous injection of NPs delivered sufficient DOX to 4T1 tumors and inhibited tumor growth. Sun et al. used 4T1 CM-coated, DOX-loaded gold nanocages (AuNCs) for a combinational chemo- and photothermal 4T1 metastatic breast cancer therapy, combining hyperthermia-responsive and tumor-targeting capabilities [3]. In another study, Sun et al.

investigated the anti-tumor and anti-metastatic efficacy of 4T1 CM-coated, paclitaxel (PTX)-loaded polymeric NPs on 4T1 primary nodules as well as metastatic nodules in the lung [1]. The intravenous injection of a CCM-coated nanoparticle (TPZ@PCN@Mem) enabled effective PDT of 4T1 tumors. It is noteworthy that TPZ@PCN@Mem showed specific source cell targeting and immune escape *in vitro* [53]. For phototheranostic agents, cancer-associated fibroblast membrane-coated NPs were used to target cancer-associated fibroblasts in the TME. CM-coated NPs showed higher accumulation in the tumor tissue than uncoated NPs and 4T1 CM-coated NPs [12]. To improve the photothermal/chemotherapy of 4T1 tumors, Wang et al. coated RBC-derived membranes onto PLGA NPs. Their study showed that RBCM-coating improved the blood circulation time, enabled immune evasion and increased the accumulation of NPs at the tumor site [51]. In conclusion, many previous studies on the design of biomimetic NPs using 4T1 CMs investigated the intravenous injection route *in vivo* [2,4,54,55]. In the present study, we intratumorally injected DOX/CS-NPs coated with RBCMs, 4T1CMs and RBC-4T1CMs into 4T1 tumor-

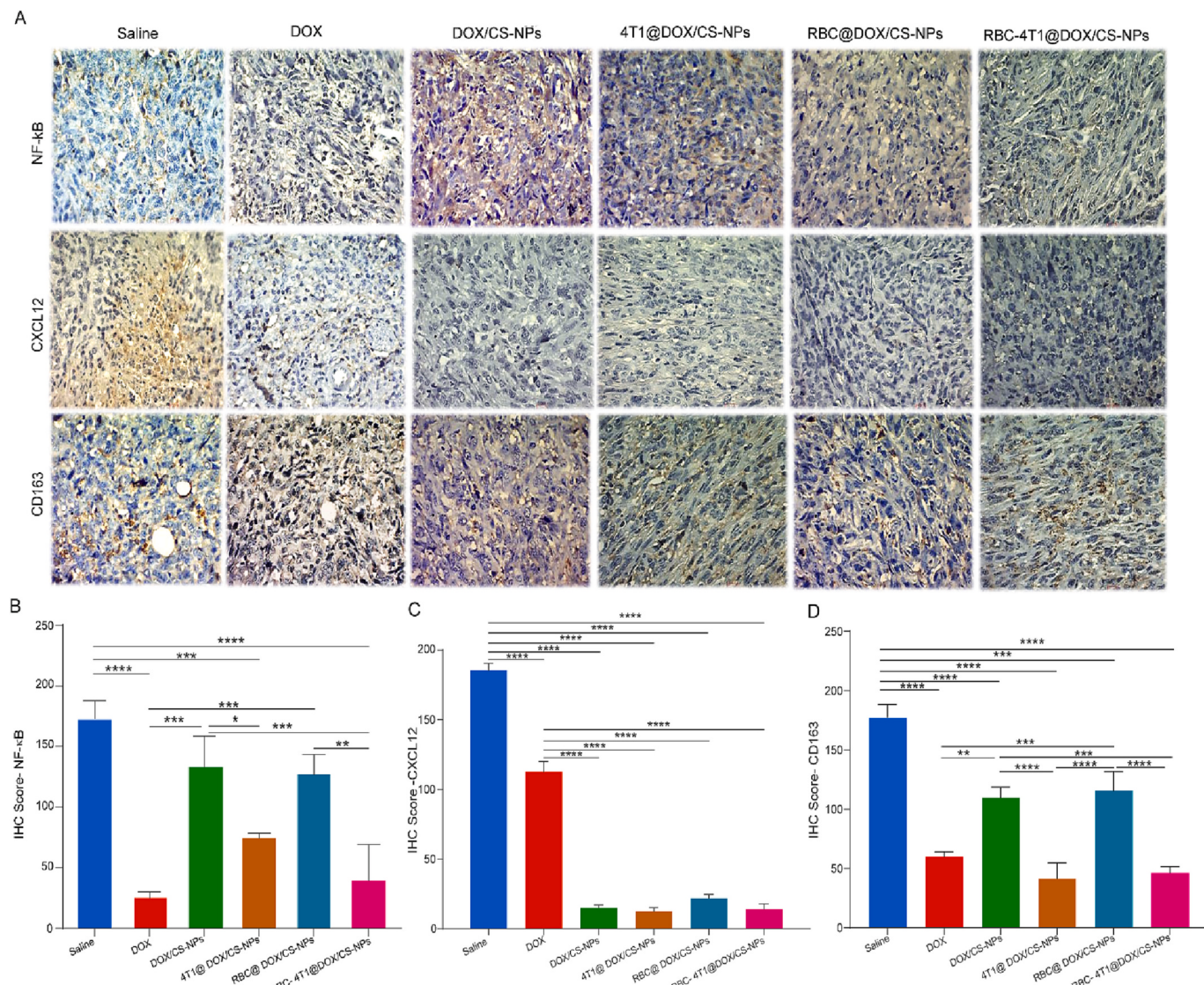


Fig. 8. Evaluation of *NfkB*, M2-TAMs (CD163) and metastatic factor (CXCL12) expression in the TME. A) The isolated tumors from treated female BALB/c were analyzed by immunohistochemistry (IHC). The immunohistological panels present images with 400 \times magnification. Images were scored and values for B) NF- κ B, C) CD163 and D) CXCL12 were plotted in the respective graph. All data are presented as mean \pm SD of six independent values ($n = 6$) per group with at least two replicates. * $p \leq 0.05$, ** $p \leq 0.01$, *** $p \leq 0.001$, **** $p \leq 0.0001$; # = ns.

bearing mice. Our results suggest the RBCMs and 4T1CMs improved the interaction of NPs with 4T1 cells in TME [56,57].

5. Conclusion

In the present study, we successfully synthesized 4T1 CM and RBCM-coated DOX/CS-NPs. In addition, we were able to fuse RBCMs with 4T1 CMs to construct an erythrocyte-cancer hybrid membrane, which was used to coat DOX/CS-NPs. After coating onto DOX/CS-NPs, the fused RBC-4T1 hybrid membrane retained both RBCM and 4T1.CM proteins. As a result, 4T1-coated DOX/CS-NPs retained their homotypic targeting properties *in vitro*. Moreover, RBCM-coated DOX/CS-NPs showed properties to escape macrophages, likely due to the high expression of CD47, which is a particular biomarker of RBC cells [38]. All membrane-coated DOX/CS-NPs showed promising tumor-homing abilities. We believe that our strategy for localized delivery of payloads could be easily applied for a wide range of solid tumors by improving the immune responses in the TME. Thus, our approach could represent a promising personalized therapy for patients in the clinic.

CRediT authorship contribution statement

S.R., L.J.C and C.E designed the experiments. S.R. performed the *in vitro* experiments. R.F.d.A.J. and I.L.G.S. performed the *in vivo* experiments. T.S. performed the TEM analysis. S.R. was responsible for most of the data and statistical analysis and drafting of the manuscript. R.F.d.A.J., C.E., T.S. and L.J.C revised the text. All authors have read and agreed to the published version of the manuscript.

Funding

L.J.C. was supported by project grants from the European Commission: Marie Skłodowska Curie grant agreement No 807281 (ACORN) and 852985 (SIMICA), C.E. was supported by the Dutch PPS allowance made available by Health~Holland, Top Sector Life Sciences and Health for the project NANOCAST 2. S.R. received funding from Marie Skłodowska Curie grant 857894 (CAST). R.F.d.A.J. was supported by project grants from CAPES [grant number 88881.119850/CNPq (grant number 301877/2019-0)]. I.L.G.S. received funding from CNPq (grant number 301877/2019-0).

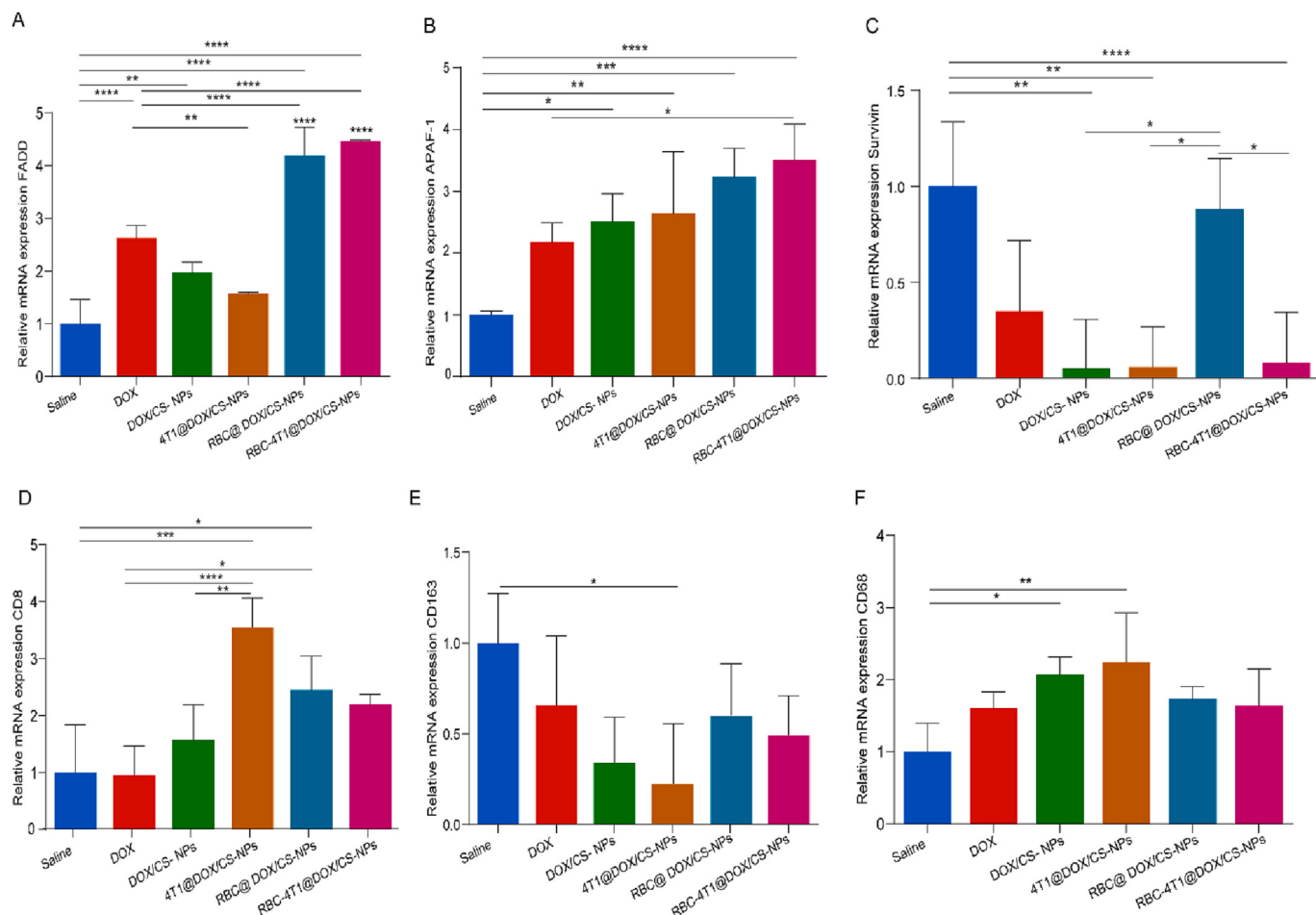


Fig. 9. Evaluation of cell death and immune response in the TME. A-G) The isolated tumors from previously treated female BALB/c analyzed for relative mRNA expression of A) *Fadd*, B) *Apaf-1*, C) *Survivin*, D) *CD8*, E) *CD163* and F) *CD68* in tumors after NP treatment. All data are presented as mean \pm SD of six independent values ($n = 5$) per group with at least two replicates. * $p < 0.05$, ** $p < 0.01$, *** $p < 0.001$, **** $p \leq 0.0001$, # = ns.

Declaration of transparency and scientific rigor

This declaration acknowledges that this paper adheres to the principles for transparent reporting and scientific rigor of preclinical research as stated in the BJP guidelines for Design & Analysis, and Animal Experimentation, and as recommended by funding agencies, publishers, and other organizations engaged with supporting research.

Informed consent statement

Not applicable.

Declaration of competing interest

No conflict of interest exists in the submission of this manuscript, and the manuscript is approved by all authors for publication.

Data availability

The original contributions presented in the study are included in the article/supplementary material. Further inquiries can be directed to the corresponding author.

Appendix A. Supplementary data

Supplementary data to this article can be found online at <https://doi.org/10.1016/j.bioadv.2023.213456>.

References

- [1] H. Sun, J. Su, Q. Meng, Q. Yin, L. Chen, W. Gu, P. Zhang, Z. Zhang, H. Yu, S. Wang, Cancer-cell-biomimetic nanoparticles for targeted therapy of homotypic tumors, *Adv. Mater.* 28 (43) (2016) 9581–9588.
- [2] W. Pan, B. Cui, P. Gao, Y. Ge, N. Li, B. Tang, A cancer cell membrane-camouflaged nanoreactor for enhanced radiotherapy against cancer metastasis, *Chem. Commun.* 56 (4) (2020) 547–550.
- [3] H. Sun, J. Su, Q. Meng, Q. Yin, L. Chen, W. Gu, Z. Zhang, H. Yu, P. Zhang, S. Wang, Cancer cell membrane-coated gold nanocages with hyperthermia-triggered drug release and homotypic target inhibit growth and metastasis of breast cancer, *Adv. Funct. Mater.* 27 (3) (2017), 1604300.
- [4] L. Han, Y. Xu, X. Guo, C. Yuan, D. Mu, Y. Xiao, Cancer cell membrane-coated biomimetic platform for targeted therapy of breast cancer in an orthotopic mouse model, *J. Biomater. Sci. Polym. Ed.* 31 (12) (2020) 1538–1551.
- [5] D. Wang, H. Dong, M. Li, Y. Cao, F. Yang, K. Zhang, W. Dai, C. Wang, X. Zhang, Erythrocyte–cancer hybrid membrane camouflaged hollow copper sulfide nanoparticles for prolonged circulation life and homotypic-targeting photothermal/chemotherapy of melanoma, *ACS Nano* 12 (6) (2018) 5241–5252.
- [6] M. Xuan, J. Shao, L. Dai, Q. He, J. Li, Macrophage cell membrane camouflaged mesoporous silica nanocapsules for in vivo cancer therapy, *Adv. Healthc. Mater.* 4 (11) (2015) 1645–1652.
- [7] D. Dehaini, X. Wei, R.H. Fang, S. Masson, P. Angsantikul, B.T. Luk, Y. Zhang, M. Ying, Y. Jiang, A.V. Kroll, Erythrocyte–platelet hybrid membrane coating for enhanced nanoparticle functionalization, *Adv. Mater.* 29 (16) (2017), 1606209.
- [8] V. Pareek, A. Bhargava, V. Bhanot, R. Gupta, N. Jain, J. Panwar, Formation and characterization of protein corona around nanoparticles: a review, *J. Nanosci. Nanotechnol.* 18 (10) (2018) 6653–6670.
- [9] Y. He, R.F. de Araújo Júnior, L.J. Cruz, C. Eich, Functionalized nanoparticles targeting tumor-associated macrophages as cancer therapy, *Pharmaceutics* 13 (10) (2021) 1670.
- [10] N. Muhamad, T. Plengsuriyakarn, K. Na-Bangchang, Application of active targeting nanoparticle delivery system for chemotherapeutic drugs and traditional/herbal medicines in cancer therapy: a systematic review, *Int. J. Nanomedicine* 13 (2018) 3921.

- [11] L.L. Bu, L. Rao, G.T. Yu, L. Chen, W.W. Deng, J.F. Liu, H. Wu, Q.F. Meng, S.S. Guo, X.Z. Zhao, Cancer stem cell-platelet hybrid membrane-coated magnetic nanoparticles for enhanced photothermal therapy of head and neck squamous cell carcinoma, *Adv. Funct. Mater.* 29 (10) (2019), 1807733.
- [12] J. Li, X. Zhen, Y. Lyu, Y. Jiang, J. Huang, K. Pu, Cell membrane coated semiconducting polymer nanoparticles for enhanced multimodal cancer phototheranostics, *ACS Nano* 12 (8) (2018) 8520–8530.
- [13] R. Tian, Z. Wang, R. Niu, H. Wang, W. Guan, J. Chang, Tumor exosome mimicking nanoparticles for tumor combinatorial chemo-photothermal therapy, *Front. Bioeng. Biotechnol.* 8 (2020) 1010.
- [14] X. Pei, X. Pan, X. Xu, X. Xu, H. Huang, Z. Wu, X. Qi, 4T1 cell membrane fragment reunited PAMAM polymer units disguised as tumor cell clusters for tumor homotypic targeting and anti-metastasis treatment, *Biomater. Sci.* 9 (4) (2021) 1325–1333.
- [15] Z. Chen, X. Chen, J. Huang, J. Wang, Z. Wang, Harnessing protein corona for biomimetic nanomedicine design, *Biomimetics* 7 (3) (2022) 126.
- [16] D.-M. Zhu, W. Xie, Y.-S. Xiao, M. Suo, M.-H. Zan, Q.-Q. Liao, X.-J. Hu, L.-B. Chen, B. Chen, W.-T. Wu, Erythrocyte membrane-coated gold nanocages for targeted photothermal and chemical cancer therapy, *Nanotechnology* 29 (8) (2018), 084002.
- [17] Y. Liu, U.K. Sukumar, M. Kanada, A. Krishnan, T.F. Massoud, R. Paulmurugan, Camouflaged hybrid cancer cell-platelet fusion membrane nanovesicles deliver therapeutic microRNAs to presentize triple-negative breast cancer to doxorubicin, *Adv. Funct. Mater.* 31 (41) (2021), 2103600.
- [18] Y. Zhao, A. Li, L. Jiang, Y. Gu, J. Liu, Hybrid membrane-coated biomimetic nanoparticles (HM@BNPs): a multifunctional nanomaterial for biomedical applications, *Biomacromolecules* 22 (8) (2021) 3149–3167.
- [19] Y. Liu, X. Wang, B. Ouyang, X. Liu, Y. Du, X. Cai, H. Guo, Z. Pang, W. Yang, S. Shen, Erythrocyte-platelet hybrid membranes coating polypyrrol nanoparticles for enhanced delivery and photothermal therapy, *J. Mater. Chem. B* 6 (43) (2018) 7033–7041.
- [20] J. Deng, W. Xu, J. Wang, Q. Li, C. Wu, L. Wu, K. Li, Q. Li, Q. Han, J. Zhu, Cancer cell membrane-coated nanogels as redox/pH dual-responsive drug carrier for tumor-targeted therapy, *J. Mater. Chem. B* 9 (38) (2021) 8031–8037.
- [21] S. Rezaei, S. Kashanian, Y. Bahrami, L.J. Cruz, M. Motiei, Redox-sensitive and hyaluronic acid-functionalized nanoparticles for improving breast cancer treatment by cytoplasmic 17 α -methyltestosterone delivery, *Molecules* 25 (5) (2020) 1181.
- [22] S. Rezaei, S. Kashanian, Y. Bahrami, H. Zhaleh, L.J. Cruz, Enhanced intracellular delivery of curcumin by chitosan-lipoic acid as reduction-responsive nanoparticles, *Curr. Pharm. Biotechnol.* 22 (5) (2021) 622–635.
- [23] B. Bahmani, H. Gong, B. Luk, K. Haushalter, E. DeTeresa, M. Previti, J. Zhou, W. Gao, J. Bui, L. Zhang, Intratumoral immunotherapy using platelet-cloaked nanoparticles enhances antitumor immunity in solid tumors, *Nat. Commun.* 12 (2021) 1999.
- [24] M. Li, H. Fang, Q. Liu, Y. Gai, L. Yuan, S. Wang, H. Li, Y. Hou, M. Gao, X. Lan, Red blood cell membrane-coated upconversion nanoparticles for pretargeted multimodality imaging of triple-negative breast cancer, *Biomater. Sci.* 8 (7) (2020) 1802–1814.
- [25] Q. Xia, Y. Zhang, Z. Li, X. Hou, N. Feng, Red blood cell membrane-camouflaged nanoparticles: a novel drug delivery system for antitumor application, *Acta Pharm. Sin. B* 9 (4) (2019) 675–689.
- [26] Y. Qu, B. Chu, X. Wei, Y. Chen, Y. Yang, D. Hu, J. Huang, F. Wang, M. Chen, Y. Zheng, Cancer-cell-biomimetic nanoparticles for targeted therapy of multiple myeloma based on bone marrow homing, *Adv. Mater.* 2107883 (2021).
- [27] L. Rao, L.L. Bu, B. Cai, J.H. Xu, A. Li, W.F. Zhang, Z.J. Sun, S.S. Guo, W. Liu, T. H. Wang, Cancer cell membrane-coated upconversion nanoprobe for highly specific tumor imaging, *Adv. Mater.* 28 (18) (2016) 3460–3466.
- [28] J. Yang, X. Zhang, C. Liu, Z. Wang, L. Deng, C. Feng, W. Tao, X. Xu, W. Cui, Biologically modified nanoparticles as theranostic bionanomaterials, *Prog. Mater. Sci.* 118 (2021), 100768.
- [29] Q. Jiang, Y. Liu, R. Guo, X. Yao, S. Sung, Z. Pang, W. Yang, Erythrocyte-cancer hybrid membrane-camouflaged melanin nanoparticles for enhancing photothermal therapy efficacy in tumors, *Biomaterials* 192 (2019) 292–308.
- [30] J. Xiong, M. Wu, J. Chen, Y. Liu, Y. Chen, G. Fan, Y. Liu, J. Cheng, Z. Wang, S. Wang, Cancer-erythrocyte hybrid membrane-camouflaged magnetic nanoparticles with enhanced photothermal-immunotherapy for ovarian cancer, *ACS Nano* 15 (12) (2021) 19756–19770.
- [31] H. Yoshikawa, K. Nishino, H. Kosako, Identification and validation of new ERK substrates by phosphoproteomic technologies including Phos-tag SDS-PAGE, *J. Proteome* 258 (2022), 104543.
- [32] D. Zhang, Z. Ye, H. Liu, X. Wang, J. Hua, Y. Ling, L. Wei, Y. Xia, S. Sun, L. Xiao, Cell membrane coated smart two-dimensional supraparticle for in vivo homotypic cancer targeting and enhanced combinational theranostics, *Nanotheranostics* 5 (3) (2021) 275.
- [33] E. Charafe-Jauffret, C. Tarpin, V.J. Bardou, F. Bertucci, C. Ginestier, A.C. Braud, B. Puig, J. Geneix, J. Hassoun, D. Birnbaum, Immunophenotypic analysis of inflammatory breast cancers: identification of an ‘inflammatory signature’, *J. Pathol.* 202 (3) (2004) 265–273.
- [34] H. Sun, Y. Zhang, Z. Zhong, Reduction-sensitive polymeric nanomedicines: an emerging multifunctional platform for targeted cancer therapy, *Adv. Drug Deliv. Rev.* 132 (2018) 16–32.
- [35] L. Xu, S. Wu, J. Wang, Cancer cell membrane-coated nanocarriers for homologous target inhibiting the growth of hepatocellular carcinoma, *J. Bioact. Compat. Polym.* 34 (1) (2019) 58–71.
- [36] Z.Y. Di Zhang, H. Liu, X. Wang, J. Hua, Y. Ling, L. Wei, Y. Xia, S. Sun, L. Xiao, Cell membrane coated smart two-dimensional supraparticle for in vivo homotypic cancer targeting and enhanced combinational theranostics, *Nanotheranostics* 5 (3) (2021) 275.
- [37] F. Li, W.-L. Chen, B.-G. You, Y. Liu, S.-D. Yang, Z.-Q. Yuan, W.-J. Zhu, J.-Z. Li, C.-X. Qu, Y.-J. Zhou, Enhanced cellular internalization and on-demand intracellular release of doxorubicin by stepwise pH-/reduction-responsive nanoparticles, *ACS Appl. Mater. Interfaces* 8 (47) (2016) 32146–32158.
- [38] J. Su, H. Sun, Q. Meng, Q. Yin, S. Tang, P. Zhang, Y. Chen, Z. Zhang, H. Yu, Y. Li, Long circulation red-blood-cell-mimetic nanoparticles with peptide-enhanced tumor penetration for simultaneously inhibiting growth and lung metastasis of breast cancer, *Adv. Funct. Mater.* 26 (8) (2016) 1243–1252.
- [39] H. Li, K. Jin, M. Luo, X. Wang, X. Zhu, X. Liu, T. Jiang, Q. Zhang, S. Wang, Z. Pang, Size dependency of circulation and biodistribution of biomimetic nanoparticles: red blood cell membrane-coated nanoparticles, *Cells* 8 (8) (2019) 881.
- [40] N.-H. Lee, S. You, A. Taghizadeh, M. Taghizadeh, H.S. Kim, Cell membrane-cloaked nanotheapeutics for targeted drug delivery, *Int. J. Mol. Sci.* 23 (4) (2022) 2223.
- [41] H. Chen, M. Zhou, Y. Zeng, T. Miao, H. Luo, Y. Tong, M. Zhao, R. Mu, J. Gu, S. Yang, Biomimetic lipopolysaccharide-free bacterial outer membrane-functionalized nanoparticles for brain-targeted drug delivery, *Adv. Sci.* 2105854 (2022).
- [42] J.-Y. Zhu, D.-W. Zheng, M.-K. Zhang, W.-Y. Yu, W.-X. Qiu, J.-J. Hu, J. Feng, X.-Z. Zhang, Preferential cancer cell self-recognition and tumor self-targeting by coating nanoparticles with homotypic cancer cell membranes, *Nano Lett.* 16 (9) (2016) 5895–5901.
- [43] Y. Lian, X. Wang, P. Guo, Y. Li, F. Raza, J. Su, M. Qiu, Erythrocyte membrane-coated arsenic trioxide-loaded sodium alginate nanoparticles for tumor therapy, *Pharmaceutics* 12 (1) (2019) 21.
- [44] H. Rajaratnam, N.S. Rasudin, S. Safuan, N.A. Abdullah, N.F. Mokhtar, W.E. M. Fuad, Passage number of 4T1 cells influences the development of tumour and the progression of metastasis in 4T1 orthotopic mice, *Malays. J. Med. Sci.* 29 (3) (2022) 30.
- [45] Z.-G. Gao, L. Tian, J. Hu, I.-S. Park, Y.H. Bae, Prevention of metastasis in a 4T1 murine breast cancer model by doxorubicin carried by folate conjugated pH sensitive polymeric micelles, *J. Control. Release* 152 (1) (2011) 84–89.
- [46] S. Lin, Y. Zheng, M. Wang, L. Zhou, Y. Zhu, Y. Deng, Y. Wu, D. Zhang, N. Li, H. Kang, Associations of CXCL12 polymorphisms with clinicopathological features in breast cancer: a case-control study, *Mol. Biol. Rep.* 49 (3) (2022) 2255–2263.
- [47] Y. Li, Z. Qin, F. Zhang, S.T. Yang, Two-color fluorescent proteins reporting survivin regulation in breast cancer cells for high throughput drug screening, *Biotechnol. Bioeng.* 119 (3) (2022) 1004–1017.
- [48] J. Zhao, J. Ruan, G. Lv, Q. Shan, Z. Fan, H. Wang, Y. Du, L. Ling, Cell membrane-based biomimetic nanosystems for advanced drug delivery in cancer therapy: a comprehensive review, *Colloids Surf. B: Biointerfaces* 112503 (2022).
- [49] L. Zhu, Y. Zhong, S. Wu, M. Yan, Y. Cao, N. Mu, G. Wang, D. Sun, W. Wu, Cell membrane camouflaged biomimetic nanoparticles: focusing on tumor theranostics, *Mater. Today Bio* 14 (2022) 100228.
- [50] N. Dhas, M.C. García, R. Kudarha, A. Pandey, A.N. Nikam, D. Gopalan, G. Fernandes, S. Soman, S. Kulkarni, R.N. Seetharam, Advancements in cell membrane camouflaged nanoparticles: a bioinspired platform for cancer therapy, *J. Control. Release* 346 (2022) 71–97.
- [51] L. Wang, S. Chen, W. Pei, B. Huang, C. Niu, Magnetically targeted erythrocyte membrane coated nanosystem for synergistic photothermal/chemotherapy of cancer, *J. Mater. Chem. B* 8 (18) (2020) 4132–4142.
- [52] W. Xu, J. Wang, Q. Li, C. Wu, L. Wu, K. Li, Q. Li, Q. Han, J. Zhu, Y. Bai, Cancer cell membrane-coated nanogels as a redox/pH dual-responsive drug carrier for tumor-targeted therapy, *J. Mater. Chem. B* 9 (38) (2021) 8031–8037.
- [53] S.-Y. Li, H. Cheng, W.-X. Qiu, L. Zhang, S.-S. Wan, J.-Y. Zeng, X.-Z. Zhang, Cancer cell membrane-coated biomimetic platform for tumor targeted photodynamic therapy and hypoxia-amplified bioreductive therapy, *Biomaterials* 142 (2017) 149–161.
- [54] C. Hu, T. Lei, Y. Wang, J. Cao, X. Yang, L. Qin, R. Liu, Y. Zhou, F. Tong, C. S. Umeshappa, Phagocyte-membrane-coated and laser-responsive nanoparticles control primary and metastatic cancer by inducing anti-tumor immunity, *Biomaterials* 255 (2020), 120159.
- [55] R. Tian, Z. Wang, R. Niu, H. Wang, W. Guan, J. Chang, Tumor exosome mimicking nanoparticles for tumor combinatorial chemo-photothermal therapy, *Front. Bioeng. Biotechnol.* (2020) 1010.
- [56] C. Tang, D. Yin, T. Liu, R. Gou, J. Fu, Q. Tang, Y. Wang, L. Zou, H. Li, Maleimide-functionalized liposomes: prolonged retention and enhanced efficacy of doxorubicin in breast cancer with low systemic toxicity, *Molecules* 27 (14) (2022) 4632.
- [57] B. Bahmani, H. Gong, B.T. Luk, K.J. Haushalter, E. DeTeresa, M. Previti, J. Zhou, W. Gao, J.D. Bui, L. Zhang, Intratumoral immunotherapy using platelet-cloaked nanoparticles enhances antitumor immunity in solid tumors, *Nat. Commun.* 12 (1) (2021) 1–12.